Aerodynamic Analysis of a Horizontal Axis Wind Turbine by use of Helical Vortex Theory

Volume I—Theory

D. R. Jeng, T. G. Keith, Jr.,
and A. Aliakbarkhanafjeh
University of Toledo

December 1982

May 1985

of in part...

Date for general release

Aerodynamic Analysis of a Horizontal Axis Wind Turbine by use of Helical Vortex Theory

Volume I—Theory

D. R. Jeng, T. G. Keith, Jr.,
and A. Aliakbarkhanafjeh
University of Toledo
Toledo, Ohio 43606

December 1982

AERODYNAMIC ANALYSIS OF A HORIZONTAL AXIS

WIND TURBINE BY USE OF HELICAL VORTEX THEORY

(VOLUME I THEORY)

by

D. R. Jeng   T. G. Keith, Jr.

and

A. Aliakbarkhanafjeh

Department of Mechanical Engineering
University of Toledo
Toledo, Ohio 43606

December 1982

CONTENTS

SUMMARY

The theoretical development of a method of analysis for prediction of the aerodynamic performance of horizontal axis wind turbines is presented in this report. The method is based on the assumption that a helical vortex emanates from each blade element. Collectively these vortices form a vortex system that extends infinitely far downstream of the blade. Velocities induced by this vortex system are found by applying the Biot-Savart law. Accordingly, this method avoids the use of any interference factors which are used in many of the momentum theories. What's more, the method can be used to predict the performance of wind turbines with a small number of blades.

The wind turbine performance of a two-bladed rotor is determined and compared to existing experimental data and to corresponding values computed from the widely used PROP code. It was found that the present method compared favorably with experimental data especially for low wind velocities.

The wind turbine performance of a single-bladed rotor is determined subject to the condition that there was no lift on the counterweight or support span. Output power for a one-bladed wind turbine was compared to that of a two-bladed machine.

1. INTRODUCTION

Over the past few years, interest in the use of windmills to produce power has grown significantly. In support of this interest, considerable research has been directed toward the measurement and prediction of wind turbine performance. The majority of the theoretical effort employed thus far is based on a variety of methods that have long been used in the calculation of propeller performance; classical momentum theory along with a number of blade-element theories have been utilized with varying degrees of success.

A computer code developed by Wilson and Walker at Oregon State University, [1], and entitled PROP, is at present widely used to determine the aerodynamic performance of horizontal axis wind turbines. This code was developed several years ago as a general purpose wind turbine performance computer program. Accordingly, PROP has a certain amount of built-in flexibility. For example, the code contains four blade tip-loss models (NASA, Prandtl, Goldstein, and no tip-loss) which can be incorporated into the performance prediction; however, the choice of which model to use is left to the user's discretion.

The PROP code is based on a modified blade element analysis called the Glauert Vortex Theory [1]. An essential assumption of this theory is that vortices originate from the rotating blades to form a helical vortex system that passes downstream. Of fundamental importance, this trailing vortex system induces velocities which alter the flow around the blades and in turn affect the forces acting on the blades. It should be noted that because of the complexity involved the induced velocities are not determined directly in the Glauert Vortex Theory. Instead, axial and radial interference factors are calculated from which the induced velocity of the vortex system on any blade element can be evaluated. The calculation of these interference factors is

simplified by assuming that the rotor has an infinite number of blades. This assumption removes the complexity associated with the periodicity of the blade flow and permits direct application of momentum theory for the evaluation of the interference velocities. However, for single and double-bladed rotors, of principal interest here, this assumption is questionable.

Users of the PROP code have frequently encountered problems with the convergence of the numerical procedure in the program. It has been found that under certain operating conditions of a wind turbine, particularly those for large tip speed ratios (generally small wind velocities), the local value of the axial interference factor can exceed a theoretically limiting value for all tip-loss models. When the axial interference factor lies in the range $1/2 \leqslant a \leqslant 1$, this state is known as a turbulence wake or vortex ring state. Under such a condition, the velocity in the fully developed wake will then reverse direction and flow back toward the rotor. Therefore, the momentum-blade element theory ceases to be valid, and it is then necessary to modify the analysis by using Glauert's empirical data. These empirical corrections have been developed for the momentum-blade element theory and discussed in some detail in [2,3], however, theoretical performance estimations in the region are suspect even when corrected by empirical methods.

Experience has also revealed from comparison of PROP code predictions with experimental data that for all blade tip-loss models, PROP results tend to underestimate measured power output both near "cut-in" and rated wind speeds.

Because of the inherent limitations with the momentum-blade element theory and because of the need to develop an analytical method for predicting the aerodynamic performance of wind turbines with a small number of blades, it was decided that a different and more complete method of anlysis was in

order. The purpose of this report is to describe the development of the method which is termed a vortex wake model.

In the analysis, the induced velocity is directly calculated by integration of the Biot-Savart law under the assumption that a filament of the trailing vortices is helical in form, extends infinitely downstream of the rotor, and has a constant diameter. It is also assumed that the helical vortex system produced at the blade is traveling downstream with a constant velocity. This velocity is equal to the value at the rotor blade, i.e., the inflow velocity through rotor's plane of rotation. This implies that the interactions between wake elements are ignored. The lifting line theory is used to model the blades.

An analysis and a computer program for predicting the aerodynamic performance of a horizontal wind turbine by using a vortex wake method has also been developed by R. H. Miller, et al [3]. The difference between that analysis and the present one is in the modeling of the circulation around the blade and in the vortex wake and in the method of integrating the Biot-Savart law to evaluate local induced velocities. In [3], the bound circulation for blade is modeled as a step function. This means that each blade is divided into a number of spanwise sections, which are, in general, of unequal length. Each blade section is then represented by a bound line vortex of constant strength. Since jump discontinuties exist in circulation between adjacent spanwise blade sections, a trailing line vortex must be generated at each of these points. These helical vortices are further approximated by a series of straight line vortex segments, each spanning an angle of $10°$ or $15°$ over which integration is performed. In the current analysis, a continuous variation of circulation in the spanwise direction is used and the integration is

performed for the whole helical vortex sheet in the trailing wake to evaluate the local induced velocities.

The method developed was found to be very flexible and is capable of accurately predicting "cut-in" speeds and wind turbine output power. The method can handle rotors having any number of blades and the blades may be arbitrarily shaped and twisted. However, this study will concentrate on one and two-bladed rotors with blade geometry appropriate to NASA wind turbines [4,5].

It should also be mentioned that, although the analysis presented in the report is limited to steady uniform flow, the technique can be readily extended to non-steady wind with shear flow and to the case of an expanding wake.

Because the method proposed herein is based on a propeller model and because PROP also is based on a number of propeller models, it was felt that a brief review of some propeller theories as applied to wind turbines was appropriate. Hence, momentum theory, blade element theory and vortex theory will all be briefly discussed in Appendix A.

In the following, the present method, which is based on the vortex theory of propellers along with Moriya's Theory [6], will be described. Discussion will be given as to how Moriya's Theory may be implemented in determining wind turbine performance. Results of a number of calculations will be compared with existing experimental data. Finally, the method will be used to predict the performance of a single-bladed rotor.

NOMENCLATURE

a	axial interference factor
a'	rotational interference factor
a_0	lift curve slope
A	magnitude of vector $(\vec{s} - \vec{r}')$
A_m	sine series coefficients
b	distance shown in Fig. A-5
b_0	lift coefficient for zero incidence
c	chord
C	matrix defined by Eq. (2-68)
C_D	drag coefficient
C_L	lift coefficient
C_p	power coefficient $[P/(1/2\rho\pi R^2 v_0^3)]$
D	drag
f	parameter defined in Eq. (A-30)
f	general functions
F	axial force or drag on wind turbine
F_c	non-dimensional axial force
F'	reduction factor
g	function defined in Eq. (2-71)
h	parameter defined as $h = r\tan\phi$
$\hat{i}$	unit vector along X axis
I	induction factor
$\hat{j}$	unit vector along Y axis
$\hat{k}$	unit vector along Z axis

k	series index
K	non-dimensional circulation distribution function
L	lift
$\dot{m}$	mass flow rate
N	number of blades
p	pressure
p_2	downstream pressure
P	power
P_E	rated electrical power
P_G	generated electrical power
P_R	power produced by rotor
Q	torque
Q_c	non-dimensional torque
r, r'	distance along the blade
R	radius of rotor
R_e	effective radius
R_L	radius defined as $R_L = R \cos\psi$
$\vec{s}$	position vector from the origin to an element of the trailing vortex filament
S	gap width between vortex sheets shown in Fig. A-5
U	velocity of airflow through rotor
u_r	radial component of velocity
u	circumferential component of velocity
$\bar{v}$	mean velocity
V_0	wind velocity
V_2	downstream velocity
w_i	induced velocity

w_0	velocity of rigid helicoidal vortex sheet
w_n	normal component of induced velocity
w_t	tangential component of induced velocity
w_x	component of induced velocity in X direction
w_y	component of induced velocity in Y direction
w_z	component of induced velocity in Z direction
W	resultant velocity
W'	undisturbed velocity
X	X axis
Y	Y axis
Z	rearward distance from the rotor, Z axis
α	angle of attack
α_e	effective angle of attack
α_g	geometric angle of attack
α_i	induced angle of attack
β	blade angle
γ	vortex strength
Γ	circulation
δ	interval around a singularity
ε	angle defined in Eq. (2-43)
$\vec{n}$	vector defined in Fig. 2-2
η	transformation variable defined in Eq. (2-74)
ϕ	pitch angle of a helixical vortex filament
θ	azimuthal variable of a helical vortex filament measured from θ_k
θ_k	angle between the X-axis and the kth blade

λ_0 speed ratio, $\dfrac{V_0}{R\Omega}$

μ speed ratio, $\dfrac{r\Omega}{V_0}$

μ' speed ratio, $\dfrac{\Omega r'}{V_0}$

μ_0 tip speed ratio, $\dfrac{\Omega R}{V_0}$

$\xi,\ \xi'$ non-dimensional distances along the blade

ξ parameter defined by Eq.(A-36)

ρ density

σ rotor solidity $[NC/(2\pi R)]$

σ_L local solidity

$\tau_0, \tau_1, \ldots$ parameters defined by Eq. (A-43) and Eq. (A-44)

ϕ' angle defined by Eq. (2-26)

Φ velocity potential

ψ coning angle

Ω rotational speed

Ω_W rotational speed imparted to the air

2.   ANALYSIS

2.1 Introduction to Vortex Theory

From ideal flow theory it may be recalled that vorticity is defined as twice the angular velocity of an element of fluid. A region containing a concentrated amount of vorticity is called a vortex and a vortex is said to have a strength equal to the circulation around the vortex area. Helmholtz theorems [7] are a set of propositions that apply to vortices and vortex mechanics. One theorem states that in an inviscid flow within which the forces are conservative and the pressure is only a function of density, rotation of fluid particles, which travel along stream lines, is permanent. From this theorem, often referred to as the vortex continuity theorem, it becomes evident that a vortex filament cannot end abruptly, and, unless the filament forms a closed path, it must extend either to infinity or to the boundaries of the fluid. Associated with a vortex filament is a velocity field that the filament generates. This velocity is commonly referred to as the induced velocity. The induced velocity can be calculated from the Biot-Savart law [8] as

$$\vec{dw_i} = \frac{\gamma}{4\pi} \ \frac{\vec{r} \ \times \ \vec{ds}}{\left|\vec{r}\right|^3} \tag{2-1}$$

where $\vec{dw_i}$ is the induced velocity due to a vortex element, of length $\vec{ds}$ and strength γ, and $\vec{r}$ is the position vector from the point at which the induced velocity is being calculated to the element of the vortex.

2.2 Vortex Theory of Propellers

The vortex theory of propellers is based on the concept that each element of the blade can be treated as a two-dimensional airfoil section

subject to a certain local resultant velocity W and that the local lift of the blade element, dL, is associated with the circulation Γ around the contour of the airfoil. The local resultant velocity is found from the vector sum of the free stream velocity, the circumferential velocity of the section and the induced flow velocity. The Kutta-Joukowski theorem [9], for each blade element, may be written

$$dL = \rho\Gamma W dr \qquad\qquad (2\text{-}2)$$

where ρ is the local density of the air and dr is the elemental blade length. In general, the circulation Γ around a blade will vary along the blade span. As the circulation changes by the amount $\dfrac{d\Gamma}{dr} dr$ between the points r and r + dr along the blade length, it follows, from the vortex continuity principle, that a trailing vortex filament of the same strength emanates from the blade element and extends infinitely far downstream of the blade. Because trailing vortices emanate from every point along the rotating blade, they form a vortex sheet of approximately helical shape. The number of such sheets is equal to the number of blades. Due to the trailing vortex sheets there is an induced velocity distribution, w_i, in the plane of rotor. This induced velocity can be used to obtain the local resultant velocity W that may in turn be used in the Kutta-Joukowski theorem to determine the lift on a blade element.

2.3 General Assumptions

The principle assumptions on which the present analysis of the aerodynamic performance of a horizontal axis wind turbine is based may be stated as follows:

1) that the air flow is incompressible and inviscid,

2) that the free stream velocity is always parallel to the rotor shaft
    centerline and uniform along the span,

3) that the relative velocity of a blade element to the airstream is
    identical to the velocity that the blade element would have were it
    placed in a two-dimensional stream with an identical relative
    velocity,

4) that the trailing vortex system is helicoidal with constant pitch
    and diameter, extending infinitely far downstream of the blade, and
    moving with a constant velocity determined at the rotor (semi-rigid
    wake), and

5) that the hub has no effect on the rotor flow.

Unlike other vortex theories e.g., Goldstein [10] and Theodorson [11]
theories, the present method of analysis, which will be termed the helical
vortex method, does not restrict the circulation along the blade to that of
an optimum distribution corresponding to a rigid helical vortex system moving
backward from the blade with constant velocity. However, like other vortex
methods, the current method does assume that slipstream expansion is of
secondary importance and thus may be neglected. Slipstream expansion is due
to the gradual decrease of axial velocity behind the rotor which is caused by
the decrease in pressure behind the rotor. The decrease in air pressure
behind a wind turbine and the increase in air pressure immediately in front
of rotor is a direct reaction of the axial force on the wind turbine. It
should be noted that the first, second and third assumptions in the preceding
list of assumptions are identical to those used in Goldstein and Theoderson
theories. Further, no hub is permissible in either of these theories; all
integrations must begin at the origin and not at the hub radius.

The physical arrangement of the problem at hand is illustrated in Fig. 2-1. The coordinate systems for the analysis are shown in Fig. 2-2. The Cartesian coordinates X, Y, and Z are fixed in a space and were chosen such that the X-Y axes form a plane of rotation and the Z-axis is the axis of rotation. Moreover, the Z coordinate is the distance measured from the rotor to a segment of trailing vortex parallel to the axis of rotation of the rotor. The second coordinate system used is a cylindrical coordinate system (r, θ, z) which is fixed to the rotating blade. The r-axis is directed along the blade span, the θ-axis measures the azimuthal angle measured from the kth blade and the z-axis is the axis of rotation. To facilitate the analysis, the blade whose induced velocity is to be calculated, is assumed to be coincident with the x-axis as shown in Fig. 2-2.

2.4 Calculation of Induced Velocity

As has been mentioned, it is assumed that the vortex filament trailing from a blade element extends infinitely far downstream of the rotor. Associated with this vortex is a velocity field, commonly referred to as the induced velocity. This velocity field can be calculated from the Biot-Savart law [8] i.e., equation (2-1). This law is stated in vector differential form as

$$d\vec{w}_i(r') = \frac{d\Gamma}{4\pi} \frac{(\vec{s} - \vec{r}') \times d\vec{n}}{\left| \vec{s} - \vec{r}' \right|^3} \tag{2-3}$$

In this equation, $d\vec{w}_i$ is the differential velocity induced at a point r' on the blade due to a segment, $d\vec{n}$, of the trailing vortex filament which had originated at a point r on the kth blade. Also $d\Gamma$, or $\frac{d\Gamma}{dr}dr$, is the change in
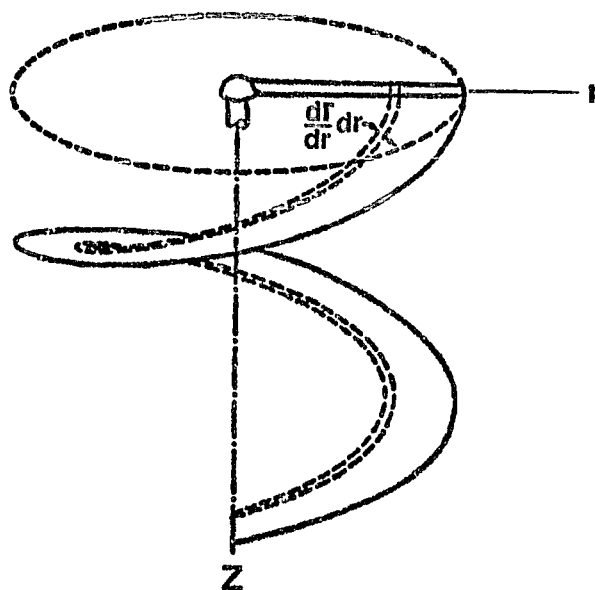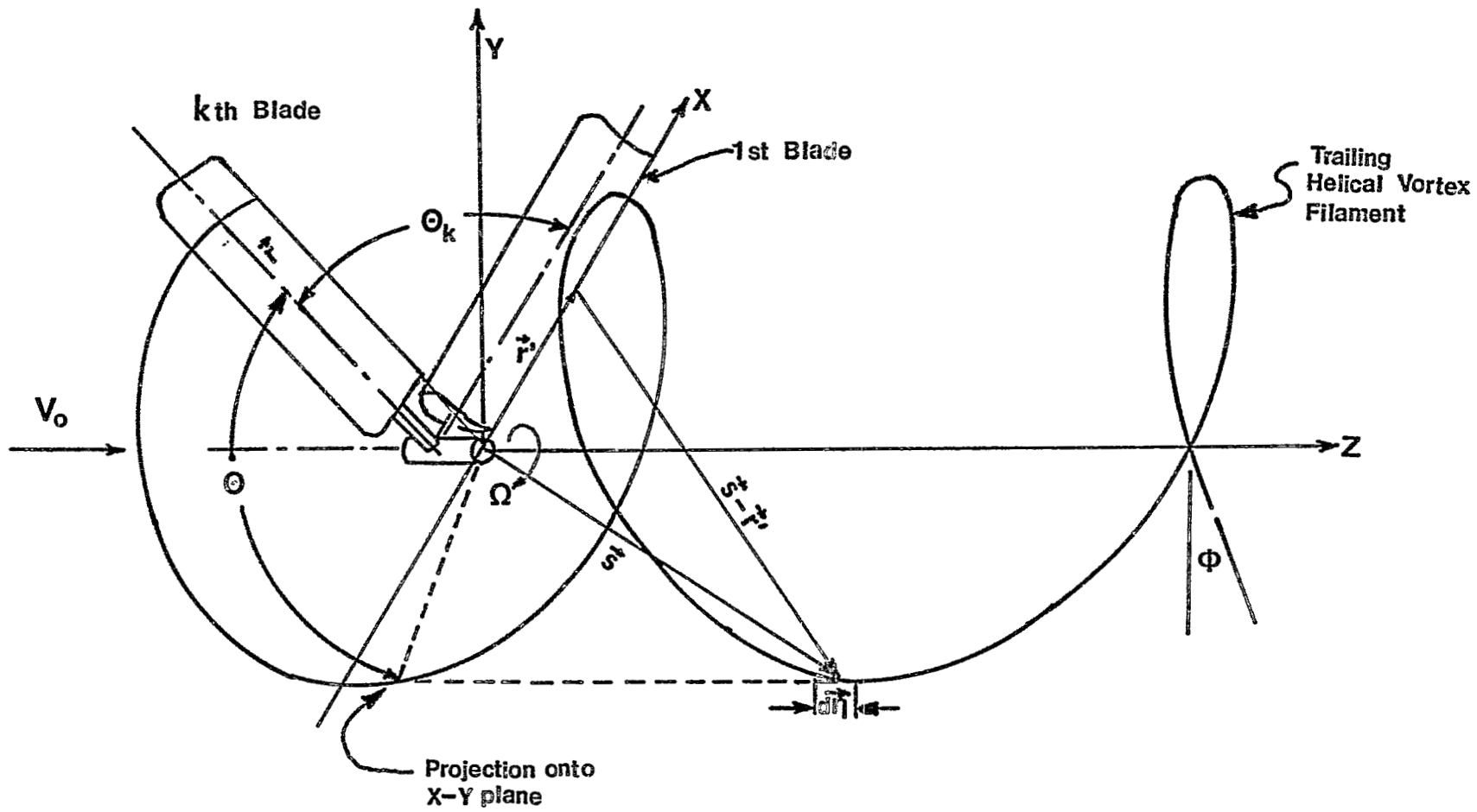
Fig. 2-1 Physical model of the problem

Fig. 2-2 Helical vortex geometry and coordinate system

circulation between the points r and r + dr along the blade, which is equal to the circulation of the trailing vortex from the blade element dr. Vectors $\vec{s}$, $\vec{r}'$, and the differential vortex filament length , $\vec{dn}$, are shown in Fig. 2-2, and may be expressed as

$$\vec{r}' = r' \; \hat{i} \tag{2-4}$$

$$\vec{s} = r \cos(\theta + \theta_k) \; \hat{i} + r \sin(\theta + \theta_k) \; \hat{j} + r\theta \tan\phi \; \hat{k} \tag{2-5}$$

$$\vec{dn} = rd\theta \; \{ \; -\sin(\theta + \theta_k) \; \hat{i} + \cos(\theta + \theta_k) \; \hat{j} + \tan\phi \; \hat{k} \; \} \tag{2-6}$$

In these expressions θ is the azimuthal angular variable of the helix measured from the kth blade and ϕ is the pitch of the helix. Both are shown in Fig. 2-2. Letting $h = r \tan\phi$ for simplicity and noting that ϕ is related to the inflow velocity U and the rotational velocity of rotor, Ω, by

$$\tan\phi = \frac{U}{r\Omega + w_y} \tag{2-7}$$

it follows that

$$h = r \tan\phi = \frac{U}{\Omega + \dfrac{w_y}{r}} \tag{2-8}$$

Thus, equations (2-5) and (2-6) may be written

$$\vec{s} = r \cos(\theta + \theta_k) \; \hat{i} + r \sin(\theta + \theta_k) \; \hat{j} + h\theta \; \hat{k} \tag{2-9}$$

$$\vec{dn} = d\theta \; \{-r \sin(\theta + \theta_k) \; \hat{i} + r \cos(\theta + \theta_k) \hat{j} + h \; \hat{k} \; \} \tag{2-10}$$

Using these equations, the cross product in the numerator of equation (2-3)

can be evaluated as follows

$$(\vec{s} - \vec{r}') \times d\vec{n} = d\theta \begin{vmatrix} \hat{i} & \hat{j} & \hat{k} \\ r\cos(\theta + \theta_k) - r' & r\sin(\theta + \theta_k) & h\theta \\ -r\sin(\theta + \theta_k) & r\cos(\theta + \theta_k) & h \end{vmatrix}$$

$$= d\theta \begin{vmatrix} r\sin(\theta + \theta_k) & h\theta \\ r\cos(\theta + \theta_k) & h \end{vmatrix} \hat{i} - d\theta \begin{vmatrix} r\cos(\theta + \theta_k) - r' & h\theta \\ -r\sin(\theta + \theta_k) & h \end{vmatrix} \hat{j}$$

$$+ d\theta \begin{vmatrix} r\cos(\theta + \theta_k) - r' & r\sin(\theta + \theta_k) \\ -r\sin(\theta + \theta_k) & r\cos(\theta + \theta_k) \end{vmatrix} \hat{k}$$

$$= d\theta\{hr[\sin(\theta + \theta_k) - \theta\cos(\theta + \theta_k)]\hat{i}$$

$$+ h[(r' - r\cos(\theta + \theta_k) - r\theta\sin(\theta + \theta_k)]\hat{j}$$

$$+ [(r^2 - rr'\cos(\theta + \theta_k)]\hat{k}\} \tag{2-11}$$

Also,

$$\left| \vec{s} - \vec{r}' \right| = (r^2 - 2rr'\cos(\theta + \theta_k) + r'^2 + h^2\theta^2)^{1/2} \tag{2-12}$$

Letting $A = \left| \vec{s} - \vec{r}' \right|$ for simplicity, noting that $d\vec{w_i}$ can be expressed in terms of its components as

$$d\vec{w_i} = dw_x \hat{i} + dw_y \hat{j} + dw_z \hat{k} \tag{2-13}$$

and combining equations (2-3), (2-11), (2-12) and (2-13), yields

$$dw_x = \frac{\dfrac{d\Gamma}{dr} \, dr}{4\pi A^3} \, hr[\sin(\theta + \theta_k) - \theta \cos(\theta + \theta_k)]d\theta \qquad (2-14)$$

$$dw_y = \frac{\dfrac{d\Gamma}{dr} \, dr}{4\pi A^3} \, h \, [r' - r \cos(\theta + \theta_k) - r\theta \sin(\theta + \theta_k)]d\theta \qquad (2-15)$$

$$dw_z = \frac{\dfrac{d\Gamma}{dr} \, dr}{4\pi A^3} \, [r^2 - rr' \cos(\theta + \theta_k)]d\theta \qquad (2-16)$$

The induced velocity components at r' due to a single helical vortex
filament that emanates from the kth blade section located a distance r along
the span can be obtained by integrating equations (2-14), (2-15) and (2-16)
with respect to θ from 0 to infinity. Now, if there are N blades, equations
(2-9), (2-10) and (2-12) become

$$\vec{s} = r \cos(\theta + \theta_k) \, \hat{i} + r \sin(\theta + \theta_k) \, \hat{j} + h\theta \, \hat{k} \qquad (2-17)$$

$$\vec{dn} = d\theta \, [-r \sin(\theta + \theta_k) \, \hat{i} + r \cos(\theta + \theta_k) \, \hat{j} + h \, \hat{k} \,] \qquad (2-18)$$

$$A = [r^2 + r'^2 - 2rr' \cos(\theta + \theta_k) + h^2\theta^2]^{1/2} \qquad (2-19)$$

where

$$\theta_k = \frac{2\pi \, (N-k)}{N} \qquad (2-20)$$

and k denotes the corresponding blade. Also, it is assumed that the blade
with k = N always coincides with the x-axis. The components of induced
velocity due to N helical vortices emanating from each blade element located
distance r from the axis of rotation are given by
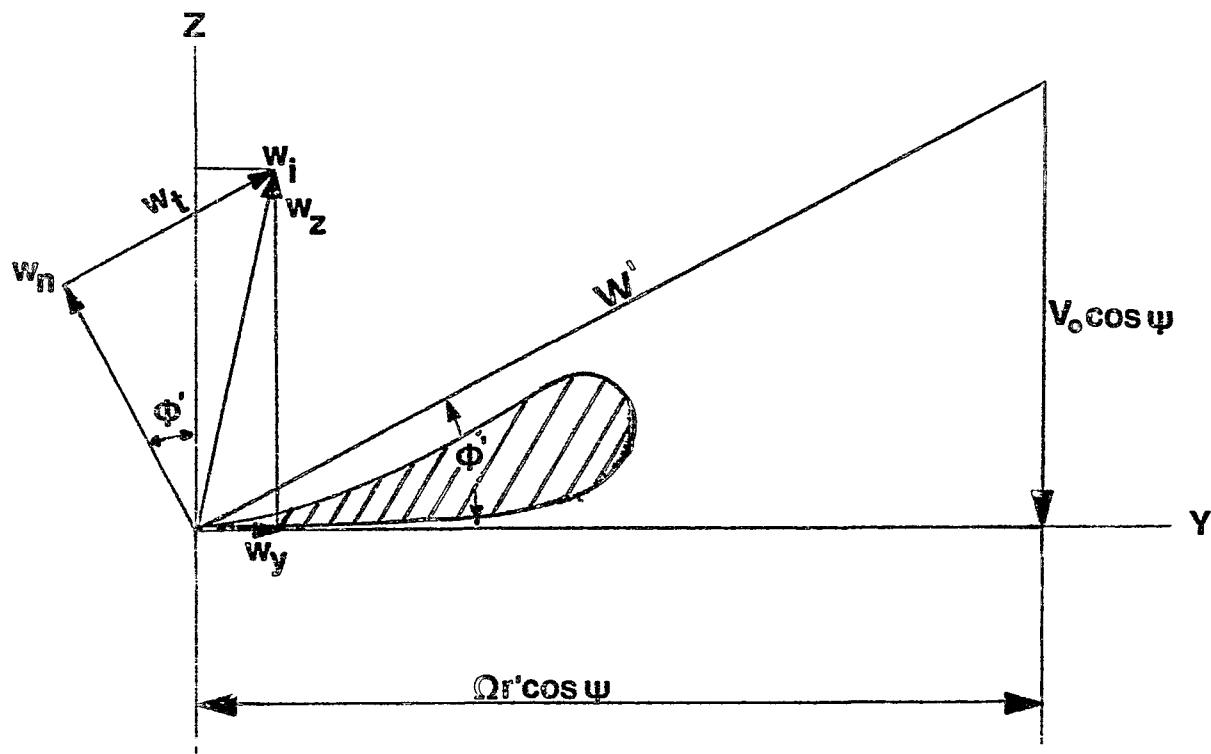
Fig. 2-3 Velocity diagram showing induced velocity and its components

$$dw_x = \frac{\frac{d\Gamma}{dr}\,dr}{4\pi} \sum_{k=1}^{N} \int_0^\infty \frac{hr\left[\sin(\theta + \theta_k) - \theta \cos(\theta + \theta_k)\right]}{A^3}\,d\theta \qquad (2\text{-}21)$$

$$dw_y = \frac{\frac{d\Gamma}{dr}\,dr}{4\pi} \sum_{k=1}^{N} \int_0^\infty \frac{h\left[r' - r\cos(\theta + \theta_k) - r\theta \sin(\theta + \theta_k)\right]}{A^3}\,d\theta \qquad (2\text{-}22)$$

$$dw_z = \frac{\frac{d\Gamma}{dr}\,dr}{4\pi} \sum_{k=1}^{N} \int_0^\infty \frac{\left[r^2 - rr'\cos(\theta + \theta_k)\right]}{A^3}\,d\theta \qquad (2\text{-}23)$$

However, $dw_x = 0$ if the diameter of the vortex helix is constant. In addition, if the induced velocity at radius r' is decomposed into directions normal and parallel to the undisturbed velocity, $\vec{W}'$, of the blade element (refer to Fig. 2-3), it may be seen that

$$dw_n = dw_z \cos\phi' - dw_y \sin\phi' \qquad (2\text{-}24)$$

$$dw_t = dw_z \sin\phi' + dw_y \cos\phi' \qquad (2\text{-}25)$$

where

$$\phi' = \tan^{-1} \frac{V_0}{r\Omega} \qquad (2\text{-}26)$$

Letting $\mu' = \dfrac{r'\Omega}{V_0}$, it is easy to show that

$$\cos\phi' = \frac{\mu'}{(\mu'^2 + 1)^{1/2}} \qquad (2\text{-}27)$$

$$\sin\phi' = \frac{1}{(\mu'^2 + 1)^{1/2}} \qquad (2\text{-}28)$$

Using these equations, the elements of induced velocity components can be

rewritten as

$$dw_n = \frac{\frac{d\Gamma}{dr}\,dr}{4\pi} \sum_{k=1}^{N} \int_0^\infty \frac{[r^2 - rr'\cos(\theta + \theta_k)]\,\mu' + h\,[r\cos(\theta + \theta_k) + }{A^3(1 + \mu'^2)^{1/2}}$$

$$\frac{r\theta\sin(\theta + \theta_k) - r']}{} \, d\theta \qquad (2\text{-}29)$$

$$dw_t = \frac{\frac{d\Gamma}{dr}\,dr}{4\pi} \sum_{k=1}^{N} \int_0^\infty \frac{[r^2 - rr'\cos(\theta + \theta_k)] - h\,[r\cos(\theta + \theta_k) + }{A^3(1 + \mu'^2)^{1/2}}$$

$$\frac{r\theta\sin(\theta + \theta_k) - r']\,\mu'}{} \, d\theta \qquad (2\text{-}30)$$

If the coning angle Ψ, shown in Fig. 2-4, is taken into account, the components of the induced velocity may be expressed as

$$dw_n = \frac{\frac{d\Gamma}{dr}\,dr}{4\pi\cos\Psi} \sum_{k=1}^{N} \int_0^\infty \frac{[r^2 - rr'\cos(\theta + \theta_k)]\,\mu' + h\,[r\cos(\theta + \theta_k) + }{A^3(1 + \mu'^2)^{1/2}}$$

$$\frac{r\theta\sin(\theta + \theta_k) - r']}{} \, d\theta \qquad (2\text{-}31)$$

$$dw_t = \frac{\frac{d\Gamma}{dr}\,dr}{4\pi\cos\Psi} \sum_{k=1}^{N} \int_0^\infty \frac{[r^2 - rr'\cos(\theta + \theta_k)] - h\,[r\cos(\theta + \theta_k) + }{A^3(1 + \mu'^2)^{1/2}}$$

$$\frac{r\theta\sin(\theta + \theta_k) - r']\,\mu'}{} \, d\theta \qquad (2\text{-}32)$$
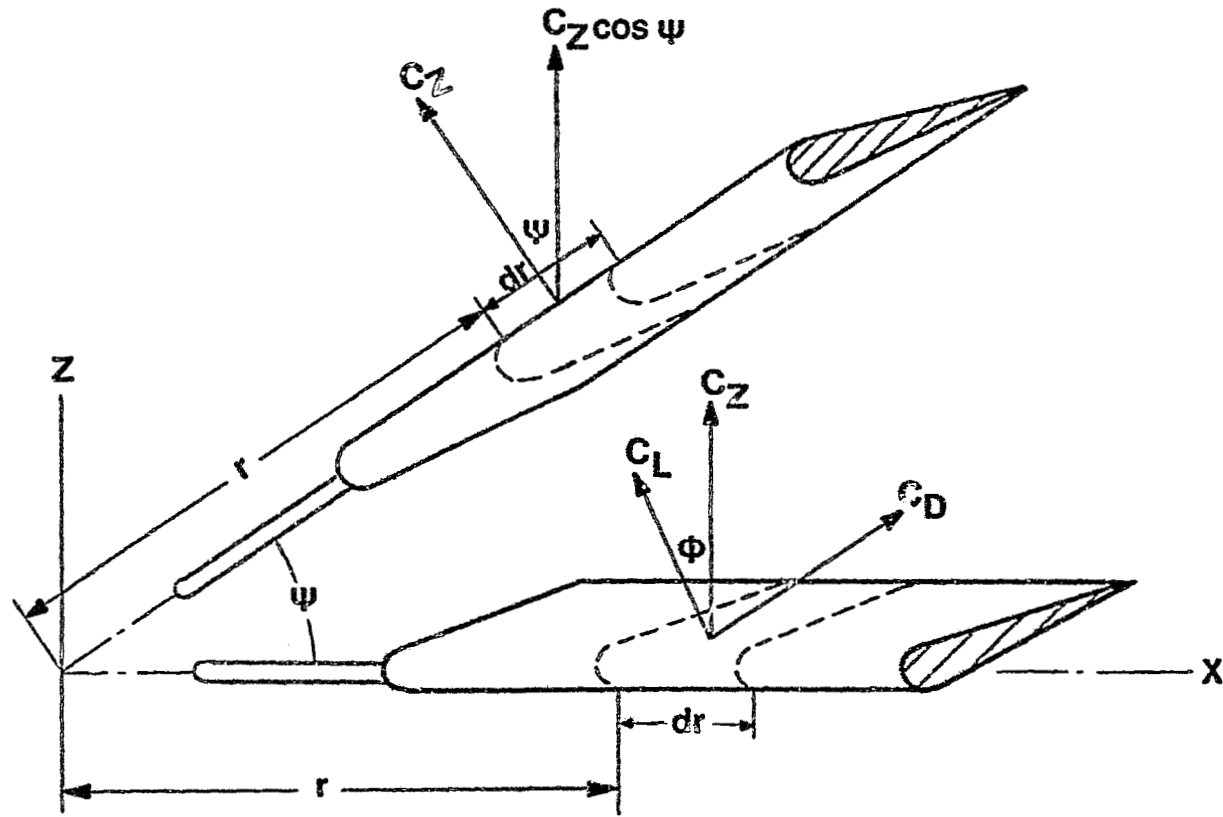
Fig. 2—4 Effect of coning angle on blade element forces

Non-dimensionalizing the distance parameters by the rotor radius R

$$\xi = \frac{r}{R} \tag{2-33}$$

$$\xi' = \frac{r'}{R} \tag{2-34}$$

and combining with equation (2-19) yields

$$A = R \left[\xi^2 - \xi'^2 - 2\xi\xi' \cos(\theta + \theta_k) + \frac{h^2}{R^2} \theta^2 \right]^{1/2} \tag{2-35}$$

Also,

$$\mu' = \frac{r'\Omega}{V_0} = \frac{r'}{R} \left(\frac{R\Omega}{V_0}\right) = \frac{\xi'}{\lambda_0} \tag{2-36}$$

and

$$(1 + \mu'^2)^{1/2} = \frac{(\lambda_0^2 + \xi'^2)^{1/2}}{\lambda_0} \tag{2-37}$$

where λ_0, the speed ratio, is defined as

$$\lambda_0 = \frac{V_0}{R\Omega} \tag{2-38}$$

By applying equations (2-33) through (2-38) to equations (2-31) and (2-32), the differential components of induced velocity can be rewritten as

$$dw_n = \frac{\frac{d\Gamma}{d\xi} d\xi}{4\pi R_L} \sum_{k=1}^{N} \int_0^\infty \frac{N_1 \xi' + N_2 \lambda_0}{D_1^{3/2} D_2^{1/2}} d\theta \tag{2-39}$$

$$dw_t = \frac{\frac{d\Gamma}{d\xi} d\xi}{4\pi R_L} \sum_{k=1}^{N} \int_0^\infty \frac{N_1 \lambda_0 - N_2 \xi'}{D_1^{3/2} D_2^{1/2}} d\theta \tag{2-40}$$

where

$$R_L = R \cos\psi$$

$$N_1 = [\xi^2 - \xi\xi' \cos(\theta + \theta_k)]$$

$$N_2 = [\xi(\theta\sin(\theta + \theta_k) + \cos(\theta + \theta_k)) - \xi'] \frac{h}{R}$$

$$D_1 = r^2 + \xi'^2 - 2\xi\xi'\cos(\theta + \theta_k) + \frac{h^2}{R^2} \theta^2$$

$$D_2 = \lambda_0^2 + \xi'^2$$

$$h = \frac{V_0 \cos\psi - w_n\cos\phi'}{\Omega \cos\psi + \dfrac{w_n\sin\phi'}{r}}$$

The total components of induced velocities can be obtained by integrating equations (2-39) and (2-40) along the blade span from the non-dimensional hub radius, ξ_{hub}, to the non-dimensional tip radius, 1. However, Moriya [6] proved that w_t is always zero at any point on the blade. Hence, the total induced velocity at point r' of the blade due to all trailing vortices originating from the blade is,

$$w_n(\xi') = \int_{\xi_{hub}}^{1} \frac{\dfrac{d\Gamma}{d\xi} d\xi}{4\pi R_L} \sum_{k=1}^{N} \int_{0}^{\infty} \frac{N_1\xi' + N_2\lambda_0}{D_1^{3/2} D_2^{1/2}} d\theta \qquad (2-41)$$

It can be seen that difficulty arises when the integral in equation (2-41) is evaluated at the point $\xi = \xi'$ when $\theta = \theta_k = 0$. In this case, the integral becomes infinitely large, and because of this singularity, the integral in equation (2-39) can not be accurately determined in the neighborhood of this particular point. However, the problem can be resolved by applying Moriya's Theory [6] which is described in the next section.

2.5 Application of Moriya's Theory

Moriya [6] has developed a simple method for determining the
downwash velocity. This was accomplished by introducing an additional
parameter to the analysis. This factor is defined as the ratio of the induced
velocity, due to a helical vortex, to the induced velocity, due to a straight
vortex, of the same strength i.e.,

$$I = \frac{dw_n}{dw_{nl}} \qquad (2\text{-}42)$$

where dw_n and dw_{nl} are induced velocities created by helical and straight
vortices respectively. The factor I is appropriately termed an induction
factor and may be considered to be a continuous function.

Induced velocity at point r' of the blade due to a helical vortex sheet
emanating from point r of the blade can be obtained from equation (2-39).
The velocity induced at point r' of the blade due to a straight vortex sheet
emanating from point r of the blade and extending infinitely far downstream
of the blade can be obtained by applying the Biot-Savart law. The following
apply for a straight vortex line

$$(\vec{s} - \vec{r}') = -(r' - r)\,\hat{i} + (r' - r)\,\tan\varepsilon\,\hat{k} \qquad (2\text{-}43)$$

$$\vec{dn} = (r' - r)\,\sec^2\varepsilon\,d\varepsilon\,\hat{k} \qquad (2\text{-}44)$$

$$\left|\vec{s} - \vec{r}'\right|^3 = \{(r' - r)\,\sec\varepsilon\}^3 \qquad (2\text{-}45)$$

In these relations, ε is the angle between the vector $(\vec{s} - \vec{r}')$ and the normal to $\vec{dn}$. Introducing equations (2-43), (2-44) and (2-45) into equation (2-1) and integrating from 0 to $\frac{\pi}{2}$, the induced velocity at the point r' of the blade due to a straight vortex line that emanates from point r of the blade and trails infinitely far downstream of the blade can be expressed as

$$dw_{n1} = \frac{\dfrac{d\Gamma}{dr}\,dr}{4\pi} \int_0^{\frac{\pi}{2}} \frac{\cos\varepsilon\; d\varepsilon}{r - r'}$$

$$= \frac{\dfrac{d\Gamma}{dr}\,dr}{4\pi} \; \frac{1}{r - r'} \tag{2-46}$$

In terms of non-dimensionalized radial distances this equation may be written

$$dw_{n1}(\xi') = \frac{\dfrac{d\Gamma}{d\xi}\,d\xi}{4\pi R} \; \frac{1}{\xi - \xi'} \tag{2-47}$$

If the blade is rotated by a coning angle ψ, equation (2-47) becomes

$$dw_{n1}(\xi') = \frac{\dfrac{d\Gamma}{d\xi}\,d\xi}{4\pi R_L} \; \frac{1}{\xi - \xi'} \tag{2-48}$$

By combining equations (2-42) and (2-48), the element of the normal induced velocity due to a helical vortex sheet originating at point r on the blade may be written as

$$dw_n(\xi') = \frac{\dfrac{d\Gamma}{d\xi}\,d\xi}{4\pi R_L} \; \frac{I}{\xi - \xi'} \tag{2-49}$$

An induction factor which is a function of ξ, ξ' and λ_0 only is derived, using equations (2-39) and (2-49), as

$$I(\xi, \xi', \lambda_0) = (\xi - \xi') \sum_{k=1}^{N} \int_0^{\infty} \frac{N_1\xi' + N_2\lambda_0}{D_1^{3/2} \, D_2^{1/2}} \, d\theta \qquad (2-50)$$

It should be pointed out that the integral in the above equation becomes infinitely large as ξ approaches ξ' and at $\theta = \theta_k = 0$. Thus, it would appear that the induction factor can not be determined with any accuracy for a small segment in the neighborhood of ξ'. However, since the induction factor is a continuous function, by virtue of its definition, it can be approximated by interpolation in the neighborhood of $\xi = \xi'$. Numerical values for the induction factor were determined by using Laguerre-Gaussian quadratures. Details of that integration may be found in volume II of this report. Having determined the distribution of the induction factor along the blade, the induced velocity at any point ξ' on the blade can be obtained by integrating equation (2-49) from the hub to the blade tip, i.e.,

$$w_n(\xi') = \int_{\xi_{hub}}^{1} \frac{\frac{d\Gamma}{d\xi}}{4\pi \, R_L} \frac{I}{\xi - \xi'} \, d\xi \qquad (2-51)$$

This integral can be numerically evaluated providing an appropriate function for circulation Γ is in hand. This step will be performed in the next two sections.

2.6 Governing Equation Formulation

The governing equation can be formulated from the fact that if the blade section is positioned at a geometric angle of attack, α_g, relative to the undisturbed incoming fluid velocity W', its setting relative to the resultant

velocity W, is α_g diminished by the downwash angle, Fig (2-5). Thus, this equation may be written as

$$\alpha_g = \alpha_e - \alpha_i \tag{2-52}$$

where α_e is effective angle of attack and α_i, the induced angle of attack. The induced angle of attack may be obtained from Fig. (2-5) as

$$\alpha_i = \tan^{-1} \frac{w_n}{W'} \tag{2-53}$$

The fact that the induced velocity, and therefore the induced angle of attack, is itself a negative number accounts for the negative sign in equation (2-52). The geometric angle of attack can be obtained from Fig. (2-5) as

$$\alpha_g = \tan^{-1} \left(\frac{\lambda_0}{\xi'}\right) - \beta \tag{2-54}$$

where β is the pitch angle of the blade element.

The induced angle of attack may be expanded in a power series in terms of $\frac{w_n}{W'}$, and, since the value of $\frac{w_n}{W'}$ is usually small, the series may be truncated after one term i.e.,

$$\alpha_i = \tan^{-1} \frac{w_n}{W'} = \frac{w_n}{W'} - \frac{(w_n/W')^3}{3} + \ldots \approx \frac{w_n}{W'}$$

But, as may be seen from Fig. (2-5)

$$W' = (V_0 \cos^2\psi + \Omega^2 r'^2 \cos^2\psi)^{1/2}$$

$$= R_L \Omega (\lambda_0^2 + \xi'^2)^{1/2}$$

Thus,

$$\alpha_i = \frac{w_n}{R_L \Omega (\lambda_0^2 + \xi'^2)^{1/2}} \tag{2-55}$$

Combining equations (2-51) and (2-55), the induced angle of attack at point
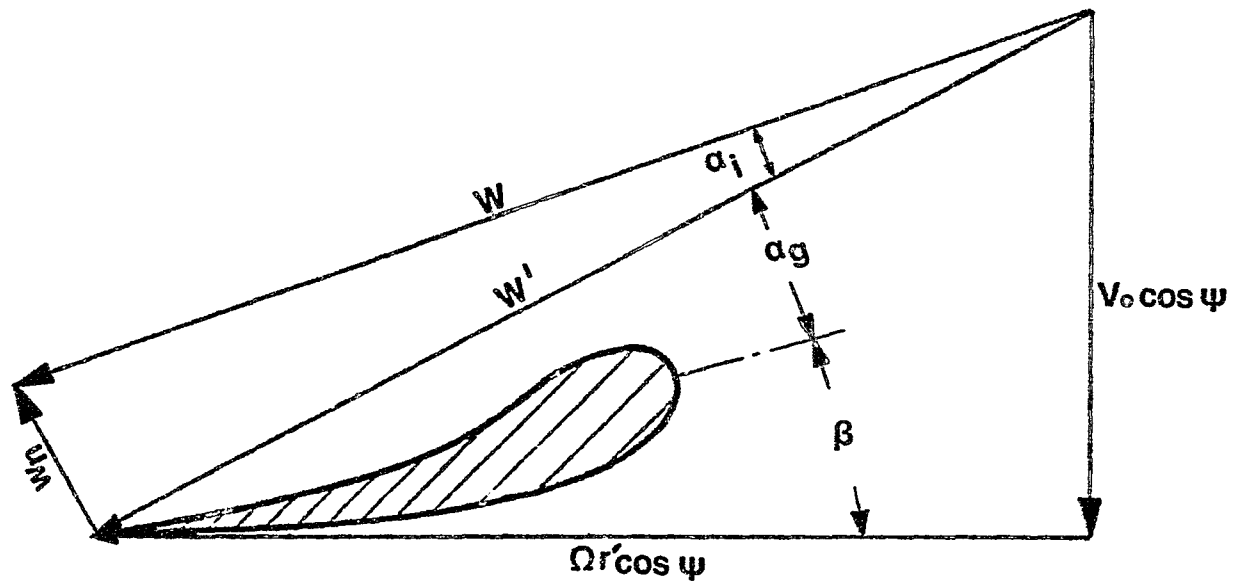
Fig. 2-5 Velocity diagram showing the effect of induced velocity

ξ' is obtained as

$$\alpha_i = \int_{\xi_{hub}}^{1} \frac{\frac{d\Gamma}{d\xi}}{4\pi R_L^2 \Omega (\lambda_0^2 + \xi'^2)^{1/2}} \frac{I}{\xi - \xi'} d\xi \tag{2-56}$$

The circulation function may be expressed as a Fourier sine series which satisfies the following boundary conditions

$$\Gamma(\xi_{hub}) = \Gamma(1) = 0 \tag{2-57}$$

A function which satisfies these boundary conditions may be written as

$$\Gamma(\xi) = \sum_{m=1}^{\infty} A_m \sin \left[(m\pi) \left(\frac{\xi - \xi_{hub}}{1 - \xi_{hub}} \right) \right] \tag{2-58}$$

The relation between circulation and lift coefficient at each section is given by Kutta-Joukowski theorem [10] as

$$\rho W \Gamma = C_L \left(\frac{1}{2} \rho W^2 \right) c$$

or

$$\Gamma = \frac{1}{2} c W C_L \tag{2-59}$$

where c is the chord of the blade section.

The section lift coefficient for an effective angle of attack can be obtained from two-dimensional airfoil data i.e.,

$$C_L = C_L (\alpha_e) \tag{2-60}$$

Furthermore, as a practical means of handling the semi-infinite series in equation (2-58), the series is truncated at M terms, (which must be the same number as the subdivision of the blade into elements).

$$\Gamma(\xi) = \sum_{m=1}^{M} A_m \sin \left[(m\pi) \left(\frac{\xi - \xi_{hub}}{1 - \xi_{hub}} \right) \right] \tag{2-61}$$

Now introducing (2-61) into (2-56) yields

$$\alpha_i = \frac{\displaystyle\sum_{m=1}^{M} mA_m \int_{\xi_{hub}}^{1} \cos\left[(m\pi)\left(\frac{\xi - \xi_{hub}}{1 - \xi_{hub}}\right)\right] \frac{I}{\xi - \xi'} d\xi}{4R_L^2\Omega(\lambda_0^2 + \xi'^2)^{1/2}(1 - \xi_{hub})} \qquad (2\text{-}62)$$

From equations (2-59), (2-60) and (2-61), and approximating the relative velocity, W, by the undisturbed velocity W' (in first iteration), the following equation may be written for any point ξ' along the blade

$$C_L(\alpha_e) = \frac{2\Gamma}{cW} \simeq \frac{2\Gamma}{cW'}$$

$$C_L(\alpha_e) = \frac{2}{cW'} \sum_{m=1}^{M} A_m \sin\left[(m\pi)\left(\frac{\xi' - \xi_{hub}}{1 - \xi_{hub}}\right)\right]$$

$$C_L(\alpha_e) = \frac{2}{c\Omega R_L(\lambda_0^2 + \xi'^2)^{1/2}} \sum_{m=1}^{M} A_m \sin\left[(m\pi)\left(\frac{\xi' - \xi_{hub}}{1 - \xi_{hub}}\right)\right] \qquad (2\text{-}63)$$

and $\quad h \simeq \dfrac{V_0}{\Omega}$ is used for the first iteration.

This equation can be regarded as a relation between α_e and the unknown circulation coefficients A_m. Thus, by substituting equation (2-63) into equation (2-52) for α_e, and making use of equation (2-62) for α_i, a single expression is obtained which allows the unknown A_m to be determined. However, it is not always possible to obtain an explicit equation for the section lift coefficient in terms of the section angle of attack from two-dimensional airfoil data. In that event, the solution must be obtained numerically.

A first approximation of the solution for α_e may be obtained by assuming a linear relation between section lift coefficient and the section effective angle of attack i.e.,

$$C_L = a_0\alpha_e + b_0 \qquad (2\text{-}64)$$

By introducing this equation into equation (2-59) and rearranging, the sectional effective angle of attack is found to be

$$\alpha_e = \frac{2\Gamma}{c_o W c} - \frac{b_0}{a_0} \tag{2-65}$$

Combining equations (2-52), (2-54) and (2-65) yields

$$\frac{2\Gamma}{a_0 W c} - \alpha_i = \frac{b_0}{a_0} + \tan^{-1}\left(\frac{\lambda_0}{\xi'}\right) - \beta \tag{2-66}$$

Now uniting equations (2-61) and (2-62) with equation (2-66) results in

$$\frac{2}{a_0 W c} \sum_{m=1}^{M} A_m \sin\left[(m\pi)\left(\frac{\xi' - \xi_{hub}}{1 - \xi_{hub}}\right)\right] -$$

$$\frac{1}{4\, R_L^2 \Omega (\lambda^2 + \xi'^2)^{1/2}\,(1 - \xi_{hub})} \sum_{m=1}^{M} m A_m \int_{\xi_{hub}}^{1} \cos\left[(m\pi)\left(\frac{\xi - \xi_{hub}}{1 - \xi_{hub}}\right)\right] \frac{I}{\xi - \xi'}\, d\xi =$$

$$\tan^{-1}\left(\frac{\lambda_0}{\xi'}\right) - \beta + \frac{b_0}{a_0} \tag{2-67}$$

Equation (2-67) is applied at M locations of ξ'. Thus, a system of M equations are obtained which may be solved for the A_m. Substituting the A_m into equation (2-61) and introducing the results into equation (2-65), produces an approximate value of α_e along the blade.

A better approximation than the above linear form may be obtained by using two-dimensional airfoil data and employing the following iteration process:

1) Use local α_e obtained from equation (2-65) for M locations along the blade to calculate the sectional C_L from two-dimensional airfoil data.

2) Calculate the local circulation Γ : $\Gamma = \frac{1}{2}\, c W C_L$.

3) Using equation (2-61) and values of Γ obtained in the second step, the following matrix equation may be established that can be used to determine A_m's.

$$[C]\ \{A\} = \{\Gamma\} \tag{2-68}$$

where

$$C_{ij} = \sin\left[(j\pi)\left(\frac{\xi'_i - \xi_{hub}}{1 - \xi_{hub}}\right)\right]$$

4) Calculate local α_i using equation (2-62)

5) Calculate a new local α_e : $\alpha_e = \alpha_g + \alpha_i$

6) Obtain C_L from two-dimensional airfoil data using the value of α_e calculated in step 5.

7) Compare the most recently calculated C_L to the previous value of C_L and if they are equal, stop the iteration, otherwise, go to step 2.

2.7 Determination of Induced Angle of Attack

The induced angle of attack can be obtained by applying equation (2-62) i.e.,

$$\alpha_i = \frac{\sum\limits_{m=1}^{M} mA_m \int\limits_{\xi_{hub}}^{1} \cos\left[(m\pi)\left(\frac{\xi - \xi_{hub}}{1 - \xi_{hub}}\right)\right] \frac{I}{(\xi - \xi')} d\xi}{4R_L^2 \Omega_0 (\lambda^2 + \xi'^2)^{1/2} (1 - \xi_{hub})} \tag{2-69}$$

However, this expression has a singularity at the point $\xi = \xi'$ and $\theta = \theta_k = 0$. To remove this singularity, the above integral is broken into three separate integrals:

$$\int\limits_{\xi_{hub}}^{1} g(\xi)\, d\xi = \int\limits_{\xi_{hub}}^{\xi'-\delta} g(\xi)d\xi + \int\limits_{\xi'-\delta}^{\xi'+\delta} g(\xi)d\xi + \int\limits_{\xi'+\delta}^{1} g(\xi)d\xi \tag{2-70}$$

where

$$g(\xi) = \frac{\cos\left[(m\pi)\left(\frac{\xi - \xi_{hub}}{1 - \xi_{hub}}\right)\right] I}{\xi - \xi'} \tag{2-71}$$

and δ is a very small number (a δ of 10^{-5} was used in the computer program).

The second integral on right hand side of equation (2-70), still contains the singularity; however, it may be given an approximate treatment as follows. The induction factor in equation (2-50) is summed over all blades. Thus, the factor may be written

$$I = I_1 + I_2 + \ldots \circ \tag{2-72}$$

where the subscripts denote the corresponding blades. Considering the particular case of two-bladed rotor, i.e., N=2, and using equation (2-71), the second integral in equation (2-70) can be rewritten as

$$\int_{\xi'-\delta}^{\xi'+\delta} \cos\left[(m\pi)\left(\frac{\xi - \xi_{hub}}{1 - \xi_{hub}}\right)\right] \frac{I}{\xi - \xi'} \, d\xi = \int_{\xi'-\delta}^{\xi'+\delta} \cos\left[(m\pi)\left(\frac{\xi - \xi_{hub}}{1 - \xi_{hub}}\right)\right] \frac{I_1}{\xi - \xi'} \, d\xi +$$

$$\int_{\xi'-\delta}^{\xi'+\delta} \cos\left[(m\pi)\left(\frac{\xi - \xi_{hub}}{1 - \xi_{hub}}\right)\right] \frac{I_2}{\xi - \xi'} \, d\xi \tag{2-73}$$

It should be noted only that the first integral in the above contains the singularity. The reason for this is that the 1st blade coincides with the X axis and contains the point $\xi = \xi'$ and $\theta = \theta_k = 0$. Making a change of variable

$$\eta = \xi - \xi' \tag{2-74}$$

allows this integral to be rewritten as

$$\int_{\xi'-\delta}^{\xi'+\delta} \cos\left[(m\pi)\left(\frac{\xi - \xi_{hub}}{1 - \xi_{hub}}\right)\right] \frac{I_1}{\xi - \xi'} \, d\xi = \int_{-\delta}^{\delta} \cos\left[(m\pi)\left(\frac{\xi' + \eta - \xi_{hub}}{1 - \xi_{hub}}\right)\right] \frac{I_1}{\eta} \, d\eta$$

The integral now can be expanded as follows

$$\int_{-\delta}^{\delta} \cos\left[(m\pi)\left(\frac{\xi' + \eta - \xi_{hub}}{1 - \xi_{hub}}\right)\right] \frac{I_1}{\eta} \, d\eta =$$

$$\cos\left[(m\pi)\left(\frac{\xi'-\xi_{hub}}{1-\xi_{hub}}\right)\right]\int_{-\delta}^{\delta}\cos\left[(m\pi)\left(\frac{\eta}{1-\xi_{hub}}\right)\right]\frac{I_1}{\eta}\,d\eta\ -$$

$$\sin\left[(m\pi)\left(\frac{\xi'-\xi_{hub}}{1-\xi_{hub}}\right)\right]\int_{-\delta}^{\delta}\sin\left[(m\pi)\left(\frac{\eta}{1-\xi_{hub}}\right)\right]\frac{I_1}{\eta}\,d\eta \qquad (2\text{-}75)$$

By expanding sine and cosine terms in power series and dropping terms of order η^2 and larger and noting that I_1 can be approximated as unity (in the region of the singularity the helical vortex appears to be straight, thus by definition ($I\approx1$) in the interval of integration, it can be shown that

$$\int_{-\delta}^{\delta}\cos\left[(m\pi)\left(\frac{\xi'+\eta-\xi_{hub}}{1-\xi_{hub}}\right)\right]\frac{I_1}{1-\xi_{hub}}\,d\eta = -\frac{2m\pi\delta}{1-\xi_{hub}}\sin\left[(m\pi)\left(\frac{\xi'-\xi_{hub}}{1-\xi_{hub}}\right)\right]$$

$$(2\text{-}76)$$

The second integral in equation (2-73) in which $\theta_k = \pi$ can be directly calculated, and hence, the induced angle of attack may be determined.

2.8 Power, Torque and Drag On a Wind Turbine

Once the iteration is successfully concluded and the effective angle of attack calculated, rotor forces and momentums and power can be calculated by applying the following equations

$$\frac{dF}{dr} = \frac{1}{2}\,\rho BcW^2(C_L\cos\phi + C_D\sin\phi)\,\cos\psi \qquad (2\text{-}77)$$

$$\frac{dQ}{dr} = \frac{1}{2}\,\rho BcW^2(C_L\sin\phi - C_D\cos\phi)r\,\cos\psi \qquad (2\text{-}78)$$

$$\frac{dP}{dr} \quad \frac{1}{2}\,\rho BcW^2(C_L\sin\phi - C_D\cos\phi)r\Omega\,\cos\psi \qquad (2\text{-}79)$$

Integration yields

$$F = \int_{\xi_{hub}}^{1} (\frac{1}{2} \rho BcW^2)(C_L\cos\phi + C_D\sin\phi)R \cos\psi \, d\xi \qquad (2\text{-}80)$$

$$Q = \int_{\xi_{hub}}^{1} (\frac{1}{2} \rho BcW^2)(C_L\sin\phi - C_D\cos\phi)R^2 \cos\psi \, \xi d\xi \qquad (2\text{-}81)$$

$$P = \int_{\xi_{hub}}^{1} (\frac{1}{2} \rho BcW^2)(C_L\sin\phi - C_D\cos\phi)R^2\Omega \cos\psi \, \xi d\xi \qquad (2\text{-}82)$$

Equations (2-77), (2-78) and (2-79) can easily be obtained from the geometry of Fig. 2-6 and noting that C_L and C_D, the section lift and drag coefficients respectively, are defined as [9]

$$C_L = \frac{dL}{1/2\rho W^2 cdr} \qquad (2\text{-}83)$$

$$C_D = \frac{dD}{1/2\rho W^2 cdr} \qquad (2\text{-}84)$$

3. RESULTS AND DISCUSSION

A digital computer program was written to perform the analysis of the preceding section. The flow diagram and the algorithm of performing the iteration procedures described in the previous section and a list of the computer programs will be presented in Volume II of this report. Results from several numerical investigations using the program will be presented for both single and double bladed machines. Computed performance data will be compared, where possible, to existing experimental data and to results obtained from the PROP code for the same operating conditions.
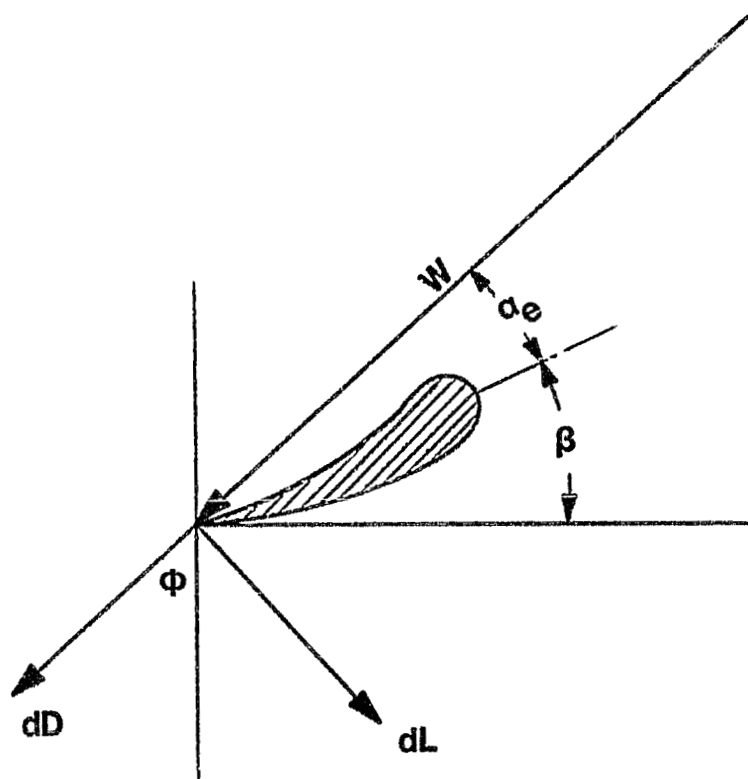
Fig. 2—6 Force components on a blade element

3.1 Double-Bladed, NACA 23024 Airfoil Wind Turbine Calculations

In this section, the power output of a double-bladed rotor wind turbine will be presented for four pitch angles and two different rotational speeds. The blade profile used in all calculations is an NACA 23024 airfoil. This particular blade section was chosen because it is the blade section used in the early NASA, large, wind turbines. Pertinent blade information is displayed in Table I. The dimensions of the blade are given in Fig. 3-1, and the aerodynamic blade data, i.e., the lift and drag coefficient curves, are shown in Figs. 3-2 and 3-3. These curves were taken from [12]. Further, because portions of the wind turbine blades may operate in the "stalled region," which occur at blade angles of attack approximately 13° and larger, the airfoil data had to be supplemented with additional information. This high angle of attack information was taken from [1]. It will be shown later in this section that better understanding of this operating region is urgently needed if improvements in performance prediction are to be realized. It should also be mentioned that surface roughness has been accounted for in Figs. 3-2 and 3-3, and that the curves correspond to a "half rough" (average between rough and smooth curves) values. The Reynolds number is that calculated at the mid span of the blade, hence, no account of the Reynolds number variation along the blade is included. Subsequent evaluations can, however, easily account for both blade surface roughness and Reynolds number effects simply by including this data as part of the computer input. At the present time, these effects were considered secondary and therefore no effort was expended to implement them in the computer program.

Circulation distribution along the blade must first be determined in order to calculate wind turbine performance. This involves evaluation of the assumed series for the circulation as described in the previous section.

A sample of the variation of this parameter against non-dimensional radius is plotted in Fig. 3-4 for the operating conditions specified.

Figure 3-5 was constructed in order to compare predicted wind turbine power output to existing experimental data. The experimental data was taken from NASA Mod-0 test results described in [4], [5] and [12]. Predicted power output values were computed for a blade fixed at a pitch angle of 0°. Experimental output data were obtained for a blade pitch angle of 0° for wind speeds below 18 mph; at wind speeds larger than 18 mph, the blades were pitched in order to maintain the rated power level of the machine.

It should be mentioned that the power output in Fig. 3-5 is not rotor power. Instead, an empirical relation, taken from [5], relating the rotor power to the alternator power has been used. This relationship accounts for the losses in the power transmission (gearing, friction, etc.) and, of course, is not applicable to all wind turbine installations. The relation is given by

$$P_G = 0.95 (P_R - 0.075P_E) \tag{3-1}$$

where

P_G = generated electrical power, kW

P_R = power produced by the rotor, kW

P_E = rated electrical power, kW

From Fig. 3-5, it can bee seen that in general there is excellent agreement between predicted and mean values of output power. Furthermore, the present method predicts a "cut-in" wind speed of 8 mph which agrees very well with the actual value reported in [4].

Figure 3-6 was drawn so as to compare predicted alternator power values of the present method to corresponding values found by using the PROP computer code. As may be seen, four models of the PROP code have been used: the Prandtl model, the Goldstein model, the no-tip-loss model and the NASA model. The theoretical background for both the Prandtl and Goldstein models is

Table 1. Operating Condition of the Utility Pole
Two-Bladed Wind Turbine

Root/Tip chord, ft	6.25/2.08
Blade Geometry	See Fig. 3-1
Percent Root Cut-Out	23%
Blade Radius, ft.	62.5
Coning Angle, Deg.	3.8
Solidity	0.033
Thickness to Chord Ratio	0.24
Airfoil	NACA 230-24
Pitch Angle, Deg.	-1, 0, +1, +3
Airfoil Surface	Rib Stitched Fiberglass Cloth
Operating, RPM	32, 33
Blade Twist	Zero
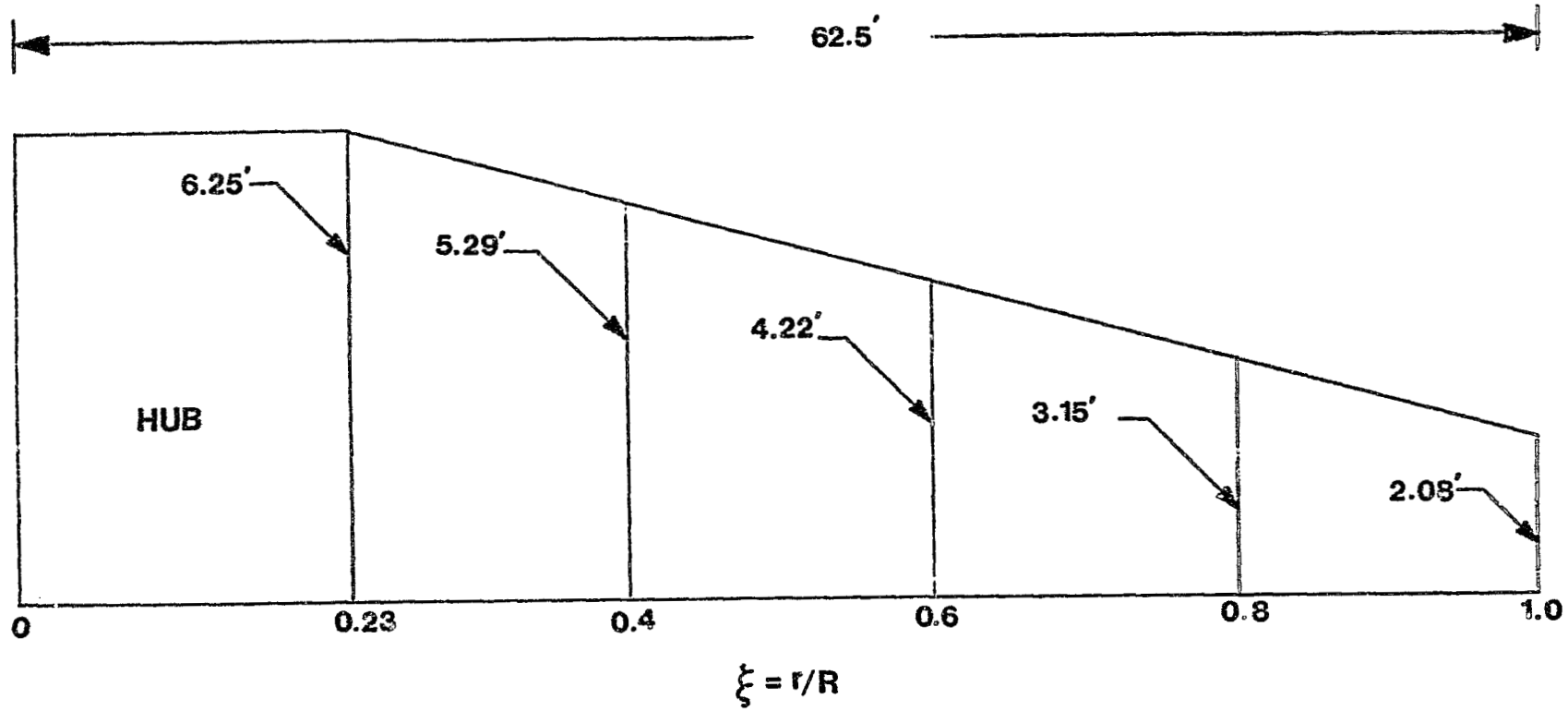
Fig. 3—1 Chord distribution along the blade
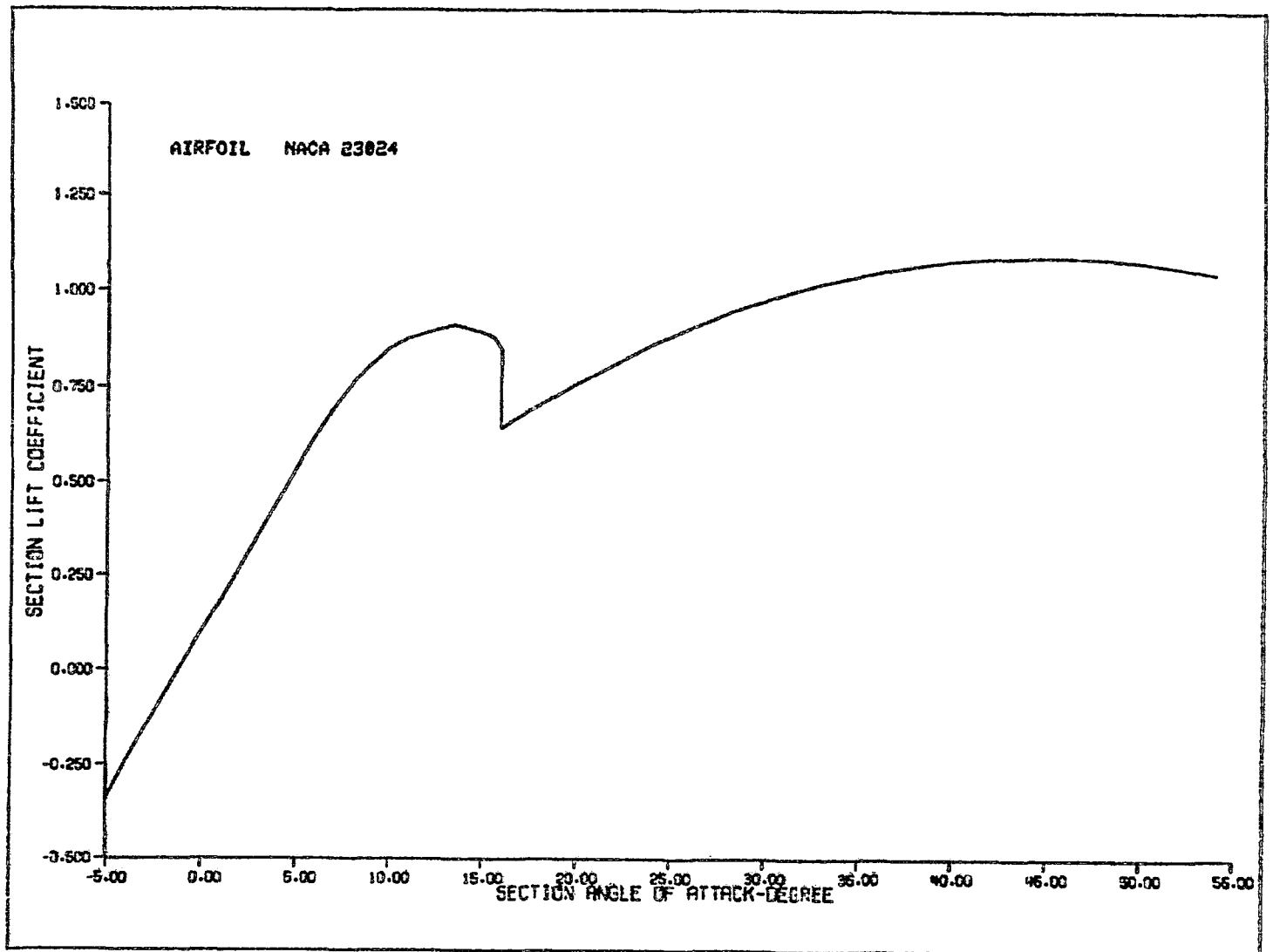
Fig. 3-2 SECTION LIFT COEFFICIENT VS. SECTION ANGLE OF ATTACK
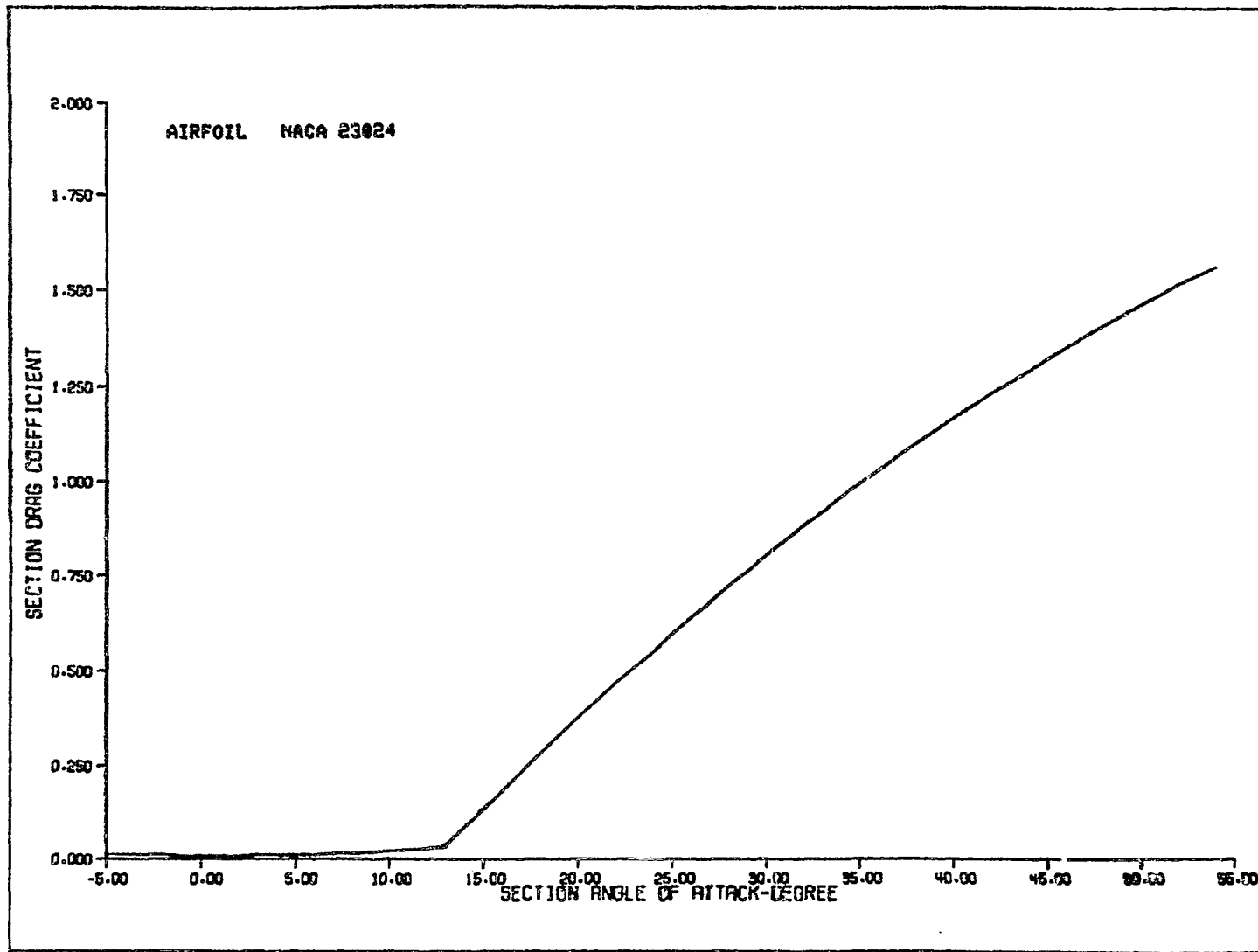
Fig. 3-3 SECTION DRAG COEFFICIENT VS. SECTION ANGLE OF ATTACK
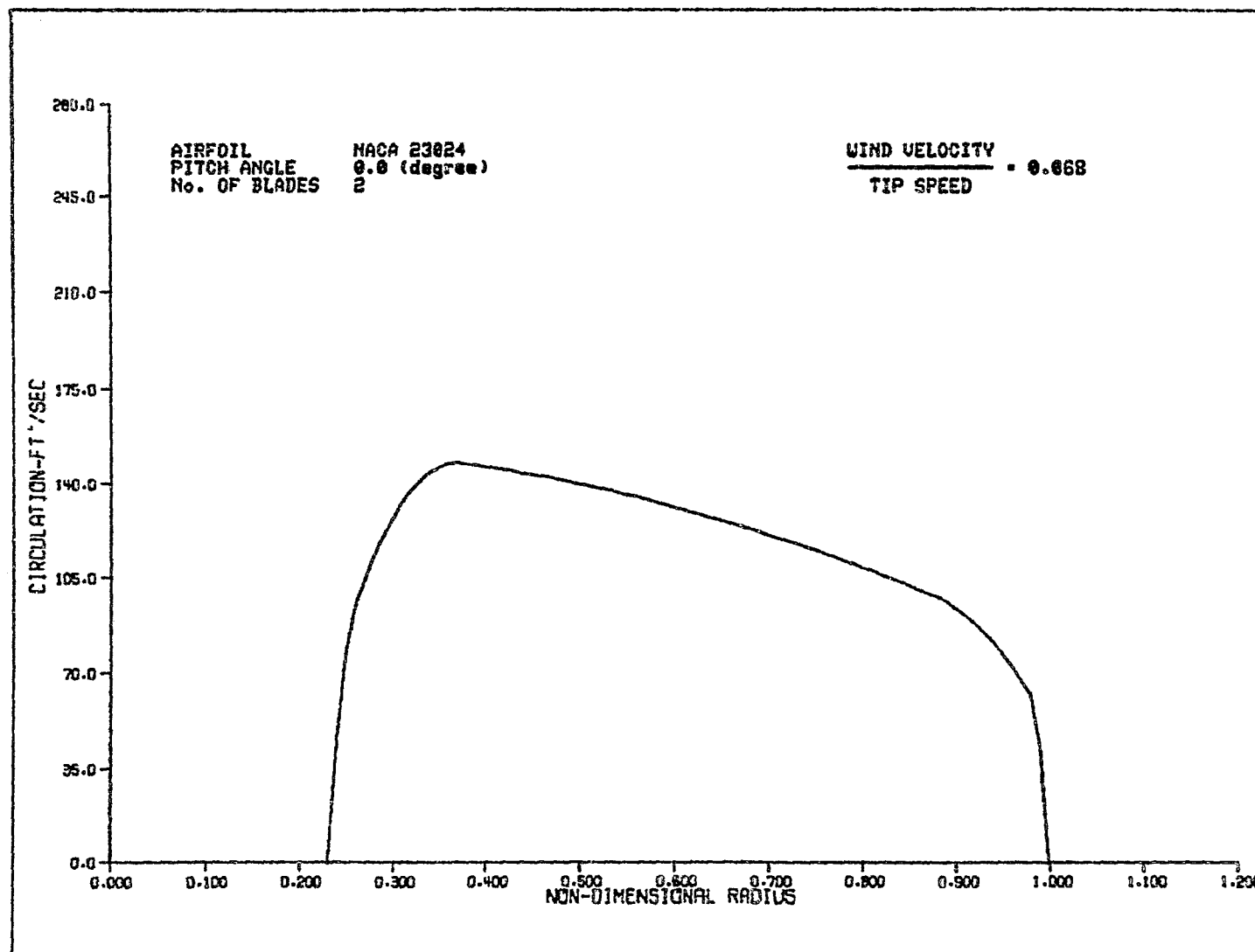
Fig. 3-4 CIRCULATION DISTRIBUTION ALONG THE BLADE
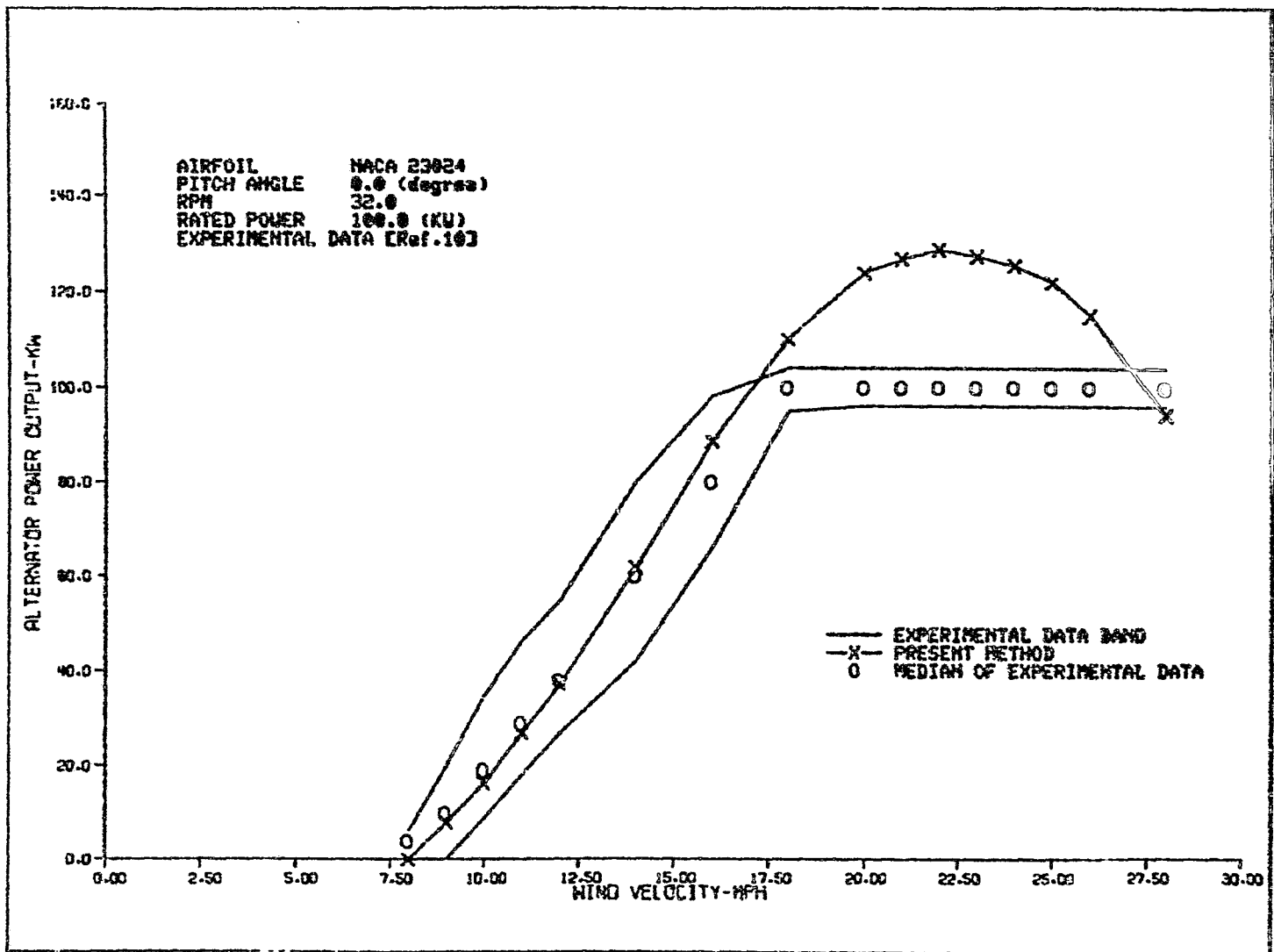
Fig. 3-5 ALTERNATOR POWER OUTPUT VS. WIND VELOCITY FOR A TWO-BLADED ROTOR
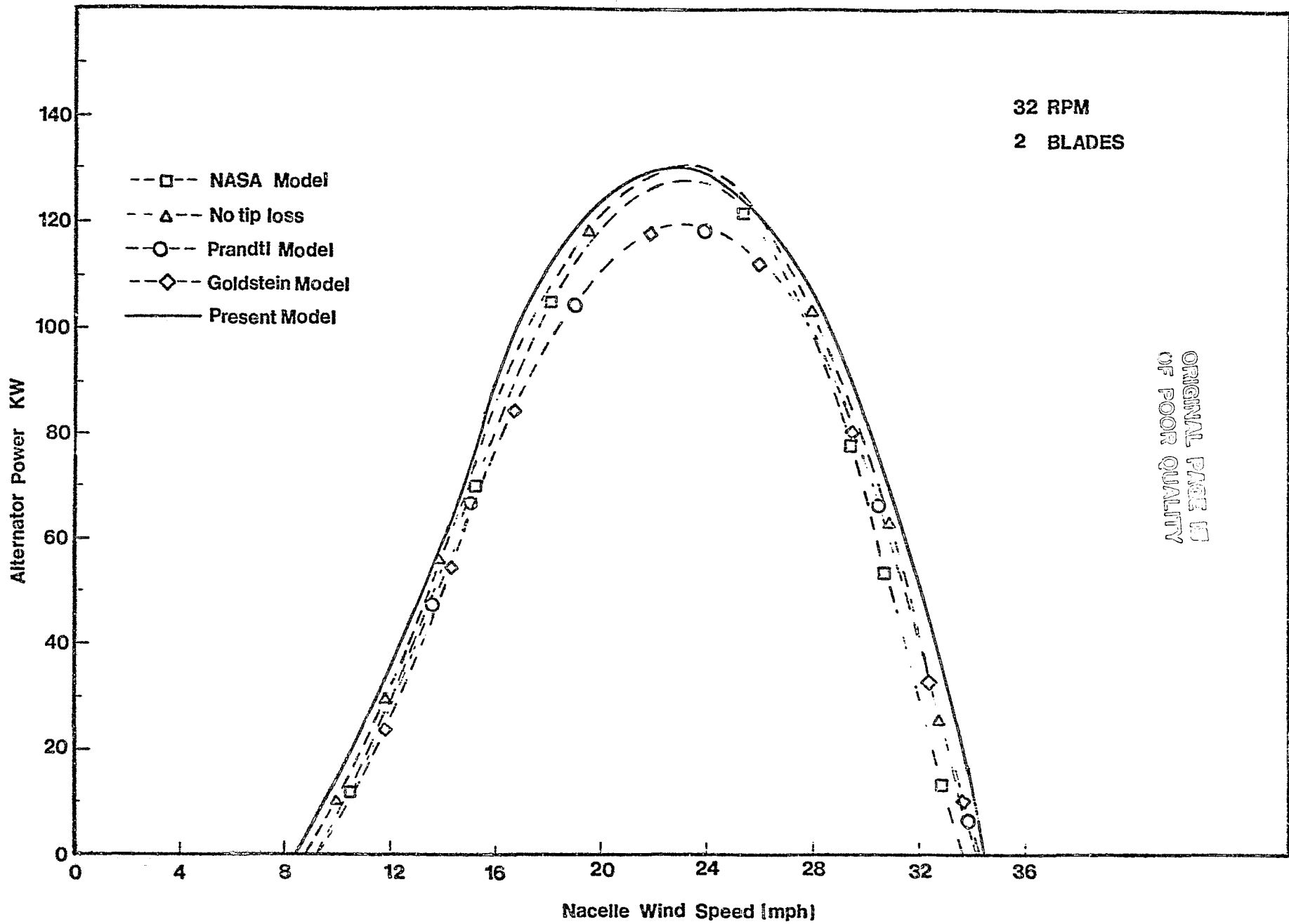
Fig. 3-6 Alternator Power v.s. Wind Speed; Zero Pitch Angle

briefly treated in Appendix A; the no-tip-loss model is self descriptive as it does not account for any blade end effects; the NASA model exploits the simplicity of the no-tip-loss model by accounting for blade end effects solely by a reduction (3%) of the blade radius -- this method is also called the effective radius model.

Reference to Fig. 3-6 shows that results determined by the present method are anywhere from 10 to 15% higher than those predicted by the PROP code for wind speeds ranging from 8 to 20 mph. These results when combined with those of Fig. 3-5 reveal that PROP code methods underestimate the power output of wind turbines in the wind speed range of interest: "cut-in" to rated. Comparison of PROP predictions with experimental data was also performed in [4] and [5]. It was found that the PROP code methods underpredicted power output and overpredicted "cut-in" wind speeds. Clearly, these findings are in total agreement with the current findings.

When existing experimental data for blade pitch angles other than 0° were compared to predicted results from both current and PROP models, it was found that agreement is not as good as that displayed in Fig. 3-5. At present, questions have been raised as to the reliability of the experimental data [13]. Thus, those comparisons will not be shown. However, it was believed that comparison between PROP prediction and current method calculations for different blade pitch angles may be of some value. This comparison is presented in the form of Tables II, III and IV where computed power output in kw is shown against wind speeds for the five methods of prediction at blade angles of -1°, +1° and +3° respectively. It must also be noted that the power values presented are rotor power values i.e., they have not been corrected by using equation (3-1). Moreover, the data are presented in tabular form because of the difficulty in graphing results that are relatively close together over various portions of the wind spectrum.

Table II. Rotor Power Vs. Wind Speed

Pitch Angle: -1°

WIND SPEED (MPH)	PRANDTL MODEL (kw)	GOLDSTEIN MODEL (kw)	NO TIP-LOSS MODEL (kw)	NASA MODEL (kw)	PRESENT MODEL (kw)
6	-1.7	-1.7	-1.9	-2.8	-7.2
8	6.3	6.3	6.2	6.0	6.5
10	15.8	15.8	17.2	16.1	25.8
12	32.3	31.3	36.3	32.3	50.0
14	61.9	60.7	68.2	61.4	77.7
16	92.3	90.7	101.1	96.1	106.6
18	116.7	115.2	128.0	124.5	126.2
20	133.4	131.8	146.5	143.6	136.7
22	141.0	139.7	152.4	152.5	137.4
24	135.9	134.9	150.3	146.6	132.8
26	123.4	123.0	135.6	130.2	113.0
28	100.4	101.2	109.6	101.9	90.0
30	68.7	70.7	73.0	62.2	69.3
32	28.4	31.9	22.4	7.2	23.5
34	-18.0	-13.2	-34.1	-61.1	-20.3
36	-67.3	-61.8	-90.1	-123.6	-53.5
38	-119.2	-113.1	-143.4	-183.1	-104.8

150	kw Rated Power
33	RPM
2	Blades
ψ	= 3.8°
23024	Airfoil

Table III. Rotor Power Vs. Wind Speed

Pitch Angle: +1°

WIND SPEED (MPH)	PRANDTL MODEL (kw)	GOLDSTEIN MODEL (kw)	NO TIP-LOSS MODEL (kw)	NASA MODEL (kw)	PRESENT MODEL (kw)
6	-8.0	-7.4	-7.1	-8.3	-6.3
8	-0.0	0.4	1.5	-0.4	4.8
10	13.7	14.0	15.9	13.3	21.0
12	34.4	34.3	37.4	34.2	42.3
14	61.7	60.1	64.8	61.7	68.2
16	90.1	86.2	92.9	90.5	97.3
18	118.1	110.4	119.5	118.8	127.8
20	141.9	131.2	142.7	142.9	147.9
22	160.5	149.0	162.4	161.4	163.2
24	172.4	159.2	173.0	172.5	169.2
26	176.9	162.4	177.0	174.7	170.7
28	172.8	157.9	172.0	167.9	170.0
30	160.1	145.7	158.0	150.9	155.8
32	139.0	126.1	134.6	124.6	129.8
34	113.4	102.6	103.7	90.3	114.1
36	77.1	69.5	65.2	46.9	72.3
38	35.0	31.8	19.6	-8.0	0.4

150 kw Rated Power
33 RPM
2 Blades
ψ = 3.8°
23024 Airfoil

Table IV. Rotor Power Vs. Wind Speed

Pitch Angle: +3°

WIND SPEED (MPH)	PRANDTL MODEL (kw)	GOLDSTEIN MODEL (kw)	NO TIP-LOSS MODEL (kw)	NASA MODEL (kw)	PRESENT MODEL (kw)
6	-10.4	-10.5	-10.7	-12.0	-9.9
8	-2.1	-2.2	-2.1	-3.5	-0.9
10	10.6	10.4	11.2	9.5	12.4
12	28.7	28.4	30.0	28.2	30.5
14	52.2	51.7	54.7	52.9	53.6
16	79.6	79.0	83.6	82.2	80.9
18	107.6	106.6	113.6	112.8	111.6
20	134.7	133.4	143.0	142.7	143.7
22	159.2	159.4	170.0	172.0	165.0
24	182.3	180.6	195.4	196.0	185.8
26	198.6	196.6	213.6	214.1	199.6
28	208.5	208.4	224.7	226.5	199.7
30	213.6	212.0	230.2	229.0	208.7
32	209.6	208.3	225.9	222.8	209.3
34	203.4	202.9	212.6	213.1	184.5
36	185.1	185.6	196.9	188.2	174.4
38	159.4	164.4	167.6	155.5	160.5

150 kw Rated Power
 33 RPM
  2 Blades
  ψ = 3.8°
23024 Airfoil

Comparing data contained in Tables II to IV reveals that the predicted maximum power output increases as the pitch angle is increased from $-1°$ to $+3°$. Figure 3-7 was drawn in order to better understand the distinction between pitch angle settings. It can be seen that the largest values of the effective angle of attack, α_e, occur for negatively pitched wind turbine blades and that the smallest α_e occurs at positive pitch angles. To obtain an idea as to how the effective angle of attack is distributed along the blade, as calculated by the present method, α_e was plotted for five locations along the blade (3/8 span, 1/2 span, 5/8 span, 3/4 span and 7/8 span) against wind velocity in Figs. 3-8 to 3-11. Each figure corresponds to a particular blade pitch angle. Reference to the four figures reveals that at any blade location, α_e increases as the wind velocity increases and that the increase is practically linear. Moreover, it can be seen by comparison that at a given blade location and wind speed, α_e decreases as the pitch angle is changed from $-1°$ to $+3°$. Thus, blades with negative pitch angles are "stalled" at lower wind velocities than are positively pitched blades.

Unfortunately the nature of this stall condition on rotating blades is not well understood at present. In particular, the effects of the centrifugal force on the boundary layer near the tip of the blade may, in fact, delay the presence of stall. It should be noted that the stall condition could be avoided, in the operating wind speed range of the wind turbine, by appropriately twisting the blade along its span. Blade twist angles may be found by applying the computational scheme developed in the preceding section.

3.2 Single-Bladed Wind Turbine Calculations

Currently a large 5MW horizontal axis wind turbine is being designed for use in Germany. What makes this work notable is that the machine has only one blade that is balanced by a large counterweight on a stubby arm as
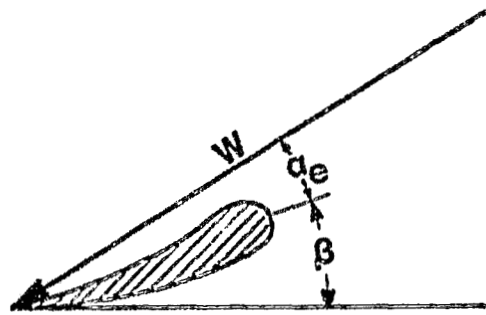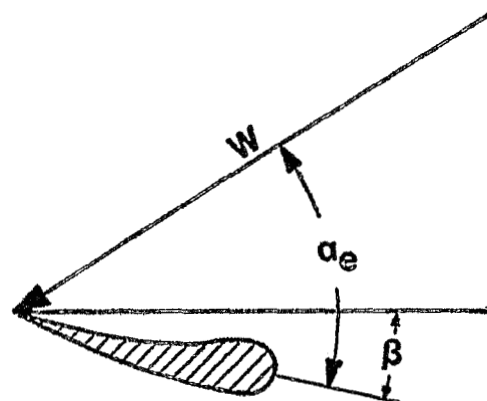
a) Positive pitch
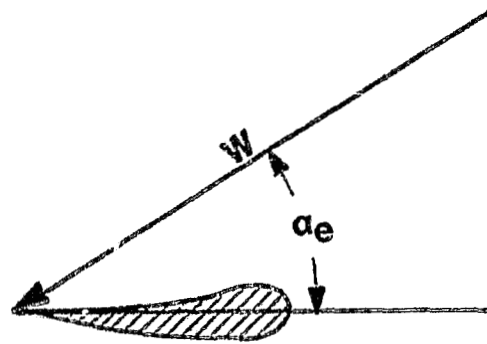
b) Zero pitch

c) Negative pitch

Fig. 3—7 Diagram showing the flow and blade angles at a blade element

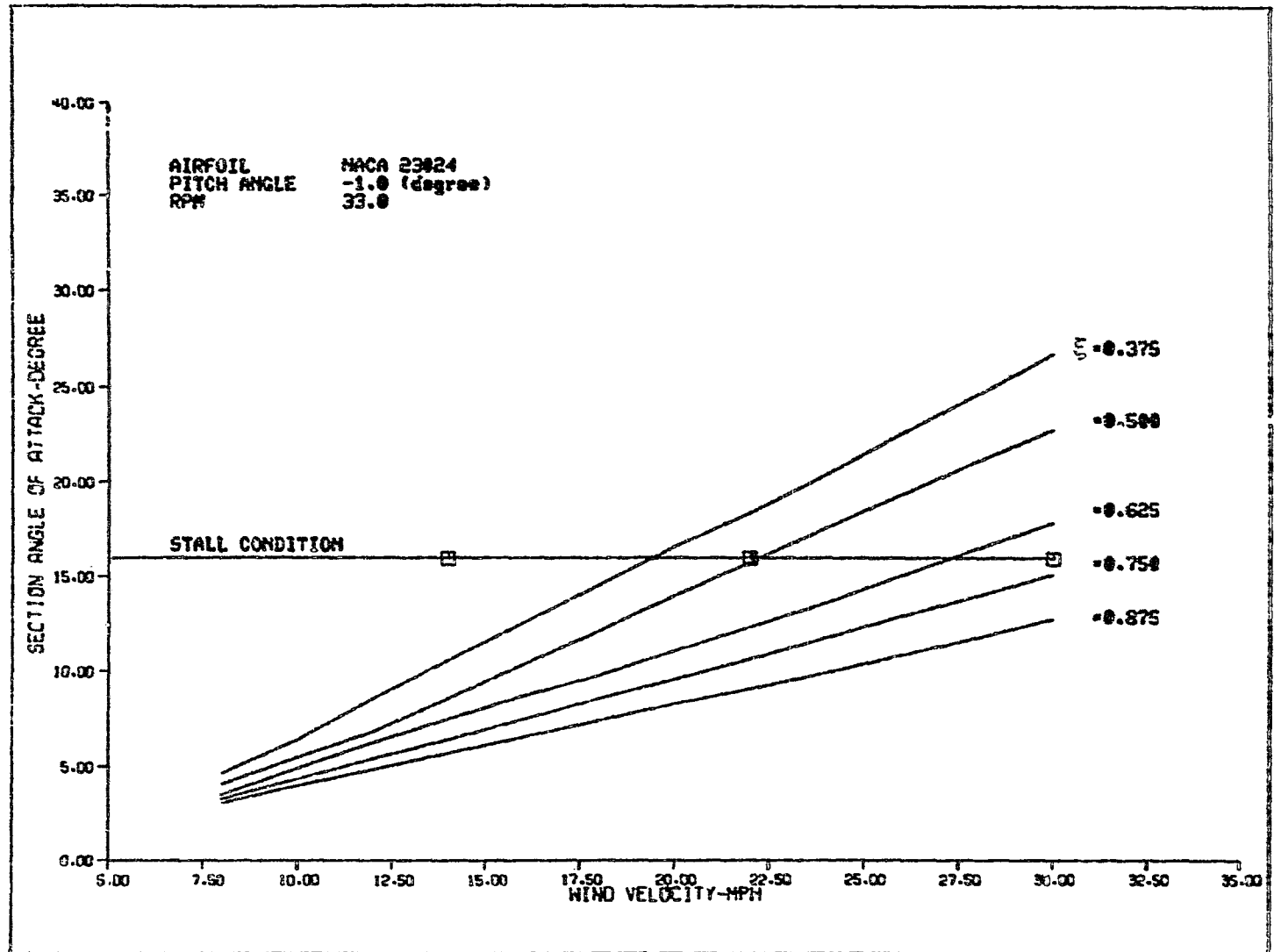Fig. 3-8 PLOT OF SECTION ANGLE OF ATTACK VS. WIND VELOCITY AT DIFFERENT
LOCATIONS ALONG THE BLADE

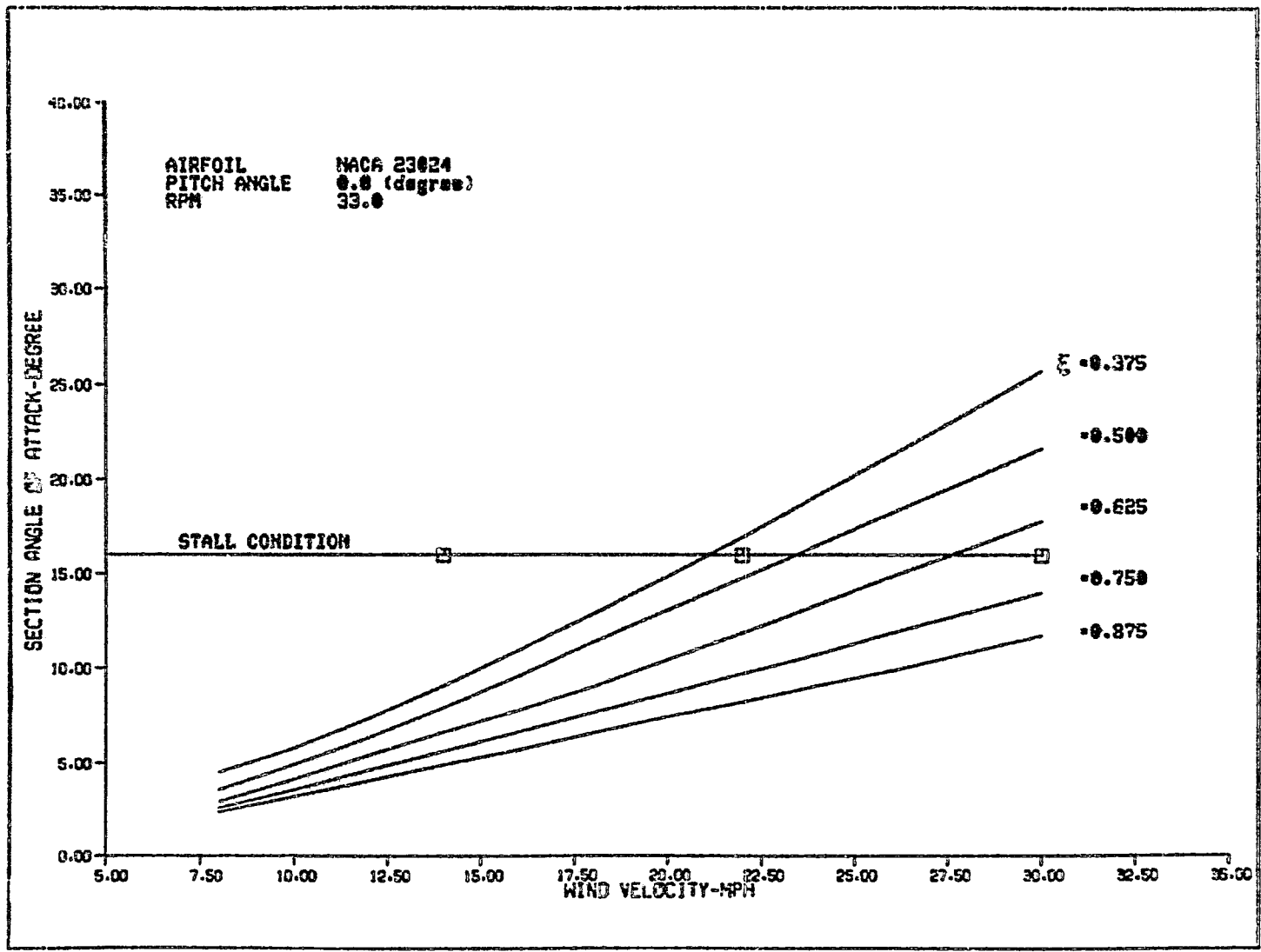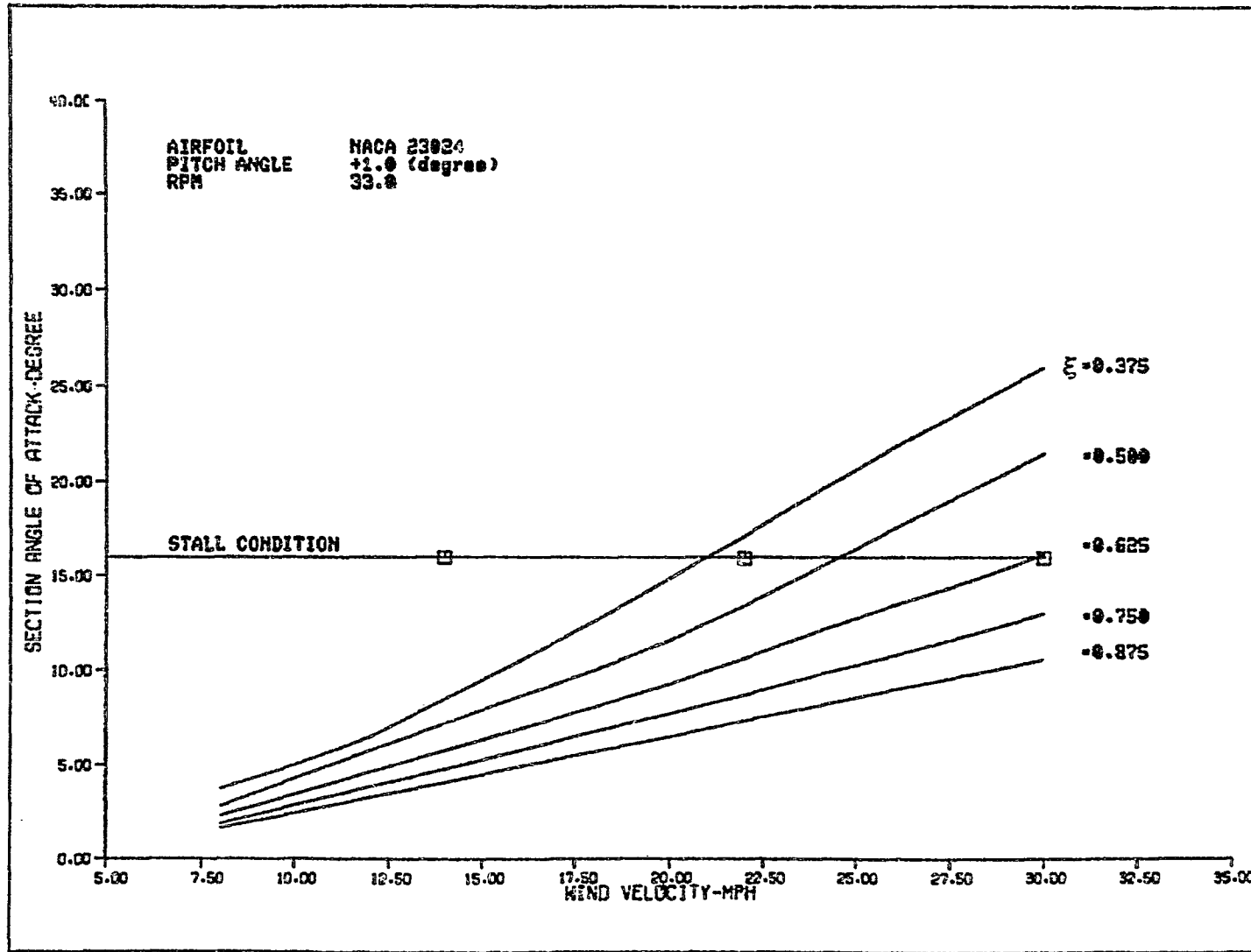Fig. 3-9 PLOT OF SECTION ANGLE OF ATTACK VS. WIND VELOCITY AT DIFFERENT LOCATIONS ALONG THE BLADE

Fig. 3-10 PLOT OF SECTION ANGLE OF ATTACK VS. WIND VELOCITY AT DIFFERENT
LOCATIONS ALONG THE BLADE
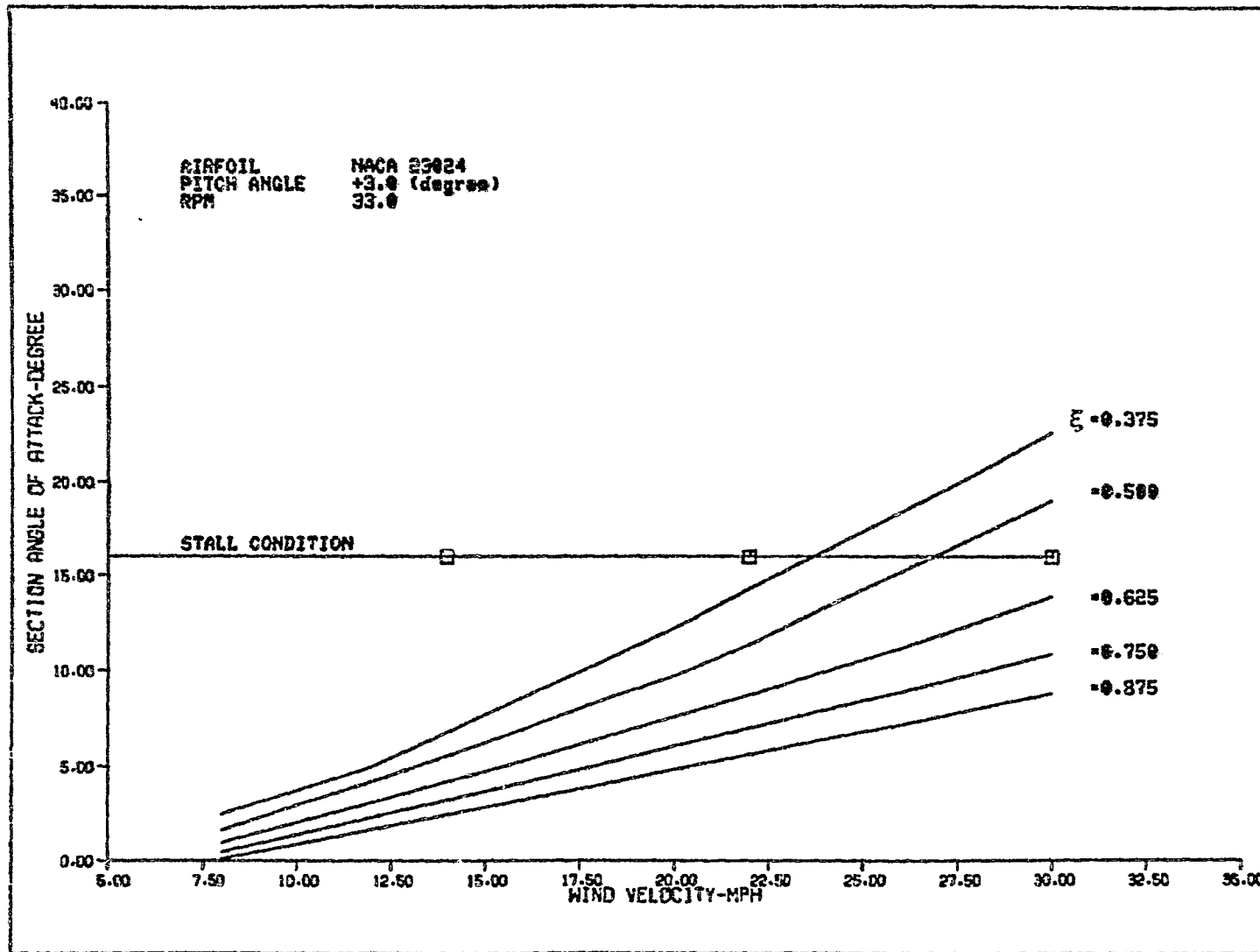
Fig. 3-11 PLOT OF SECTION ANGLE OF ATTACK VS. WIND VELOCITY AT DIFFERENT LOCATIONS ALONG THE BLADE

depicted in Fig. 3-12. It is believed that for very large wind turbines the use of a single blade reduces capital costs without much reduction in aerodynamic efficiency.

To test this premise, the computer program was used to compute the aerodynamic performance of a particular one-bladed machine. In the analyses, the counterweight was taken to be 2400 lbs and located at a radial position 25 feet from the turbine rotational axis. The counterweight and cylindrical support spar are shown in Fig. 3-13. Calculation of counterweight effect on the performance was based on the assumptions that there is no circulation around the counterweight or support spar and that the drag coefficients for these parts are 1 and 0.5 respectively.

Performance of a one-bladed and a two-bladed rotor are compared in Figs. 3-14 and 3-15. It can be seen that at 22 mph both machines produce their maximum power. However, the one-bladed machine produces less than half as much power as the two-bladed machine. Furthermore, Fig. 3-15 reveals that the two-bladed machine is also more efficient. Clearly, rotor power of a one-bladed rotor can be increased, as shown in Fig. 3-16, by operating at higher rotational velocity. This, of course, would be accomplished at the cost of higher start-up or "cut-in" speed.

Inspection of Figs. 3-14, 3-15, and 3-16 reveals that they are not sufficient to decide whether a single-bladed rotor wind turbine is practical or not. The feasibility of this concept strongly depends on the local annual wind distribution. With such wind statistical data, local annual power output of a one-bladed rotor could be estimated. It should be mentioned that the same annual power of a two-bladed wind turbine may be obtained for a one-bladed turbine if diameter of this turbine is appropriately increased.
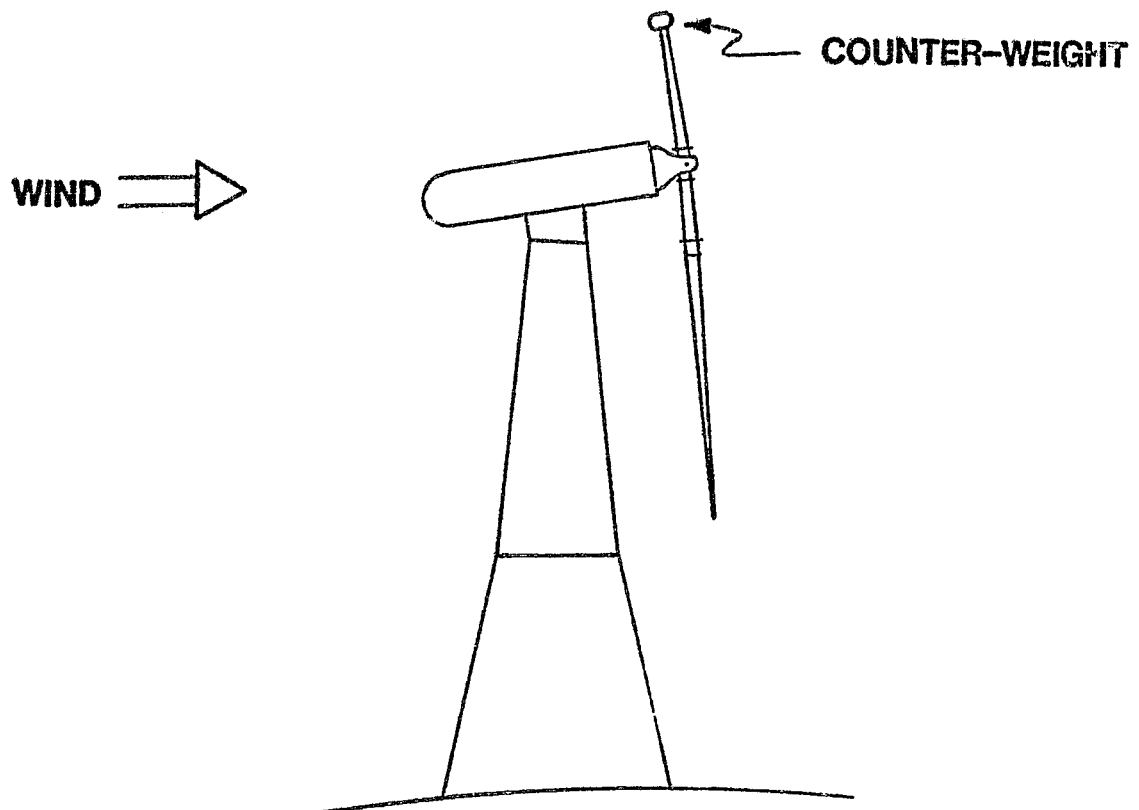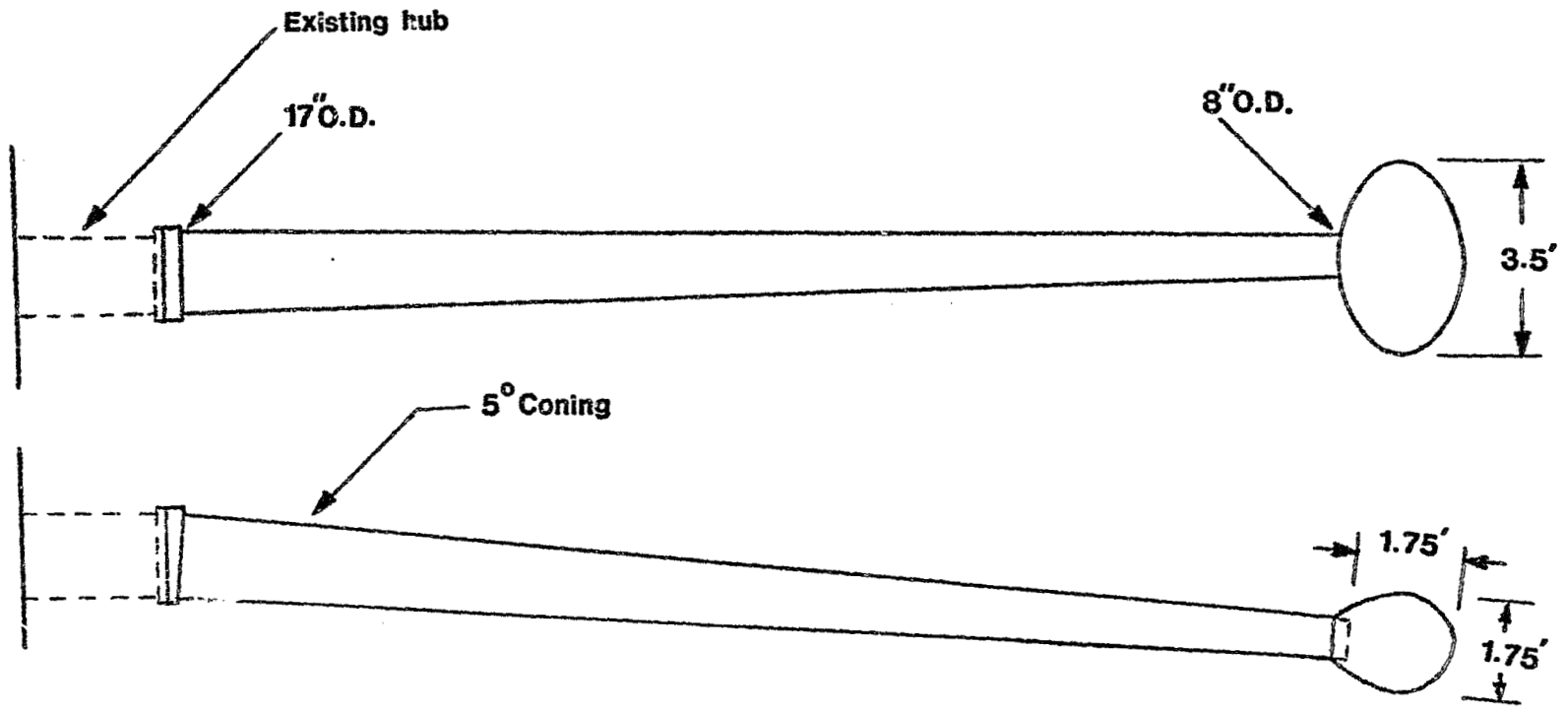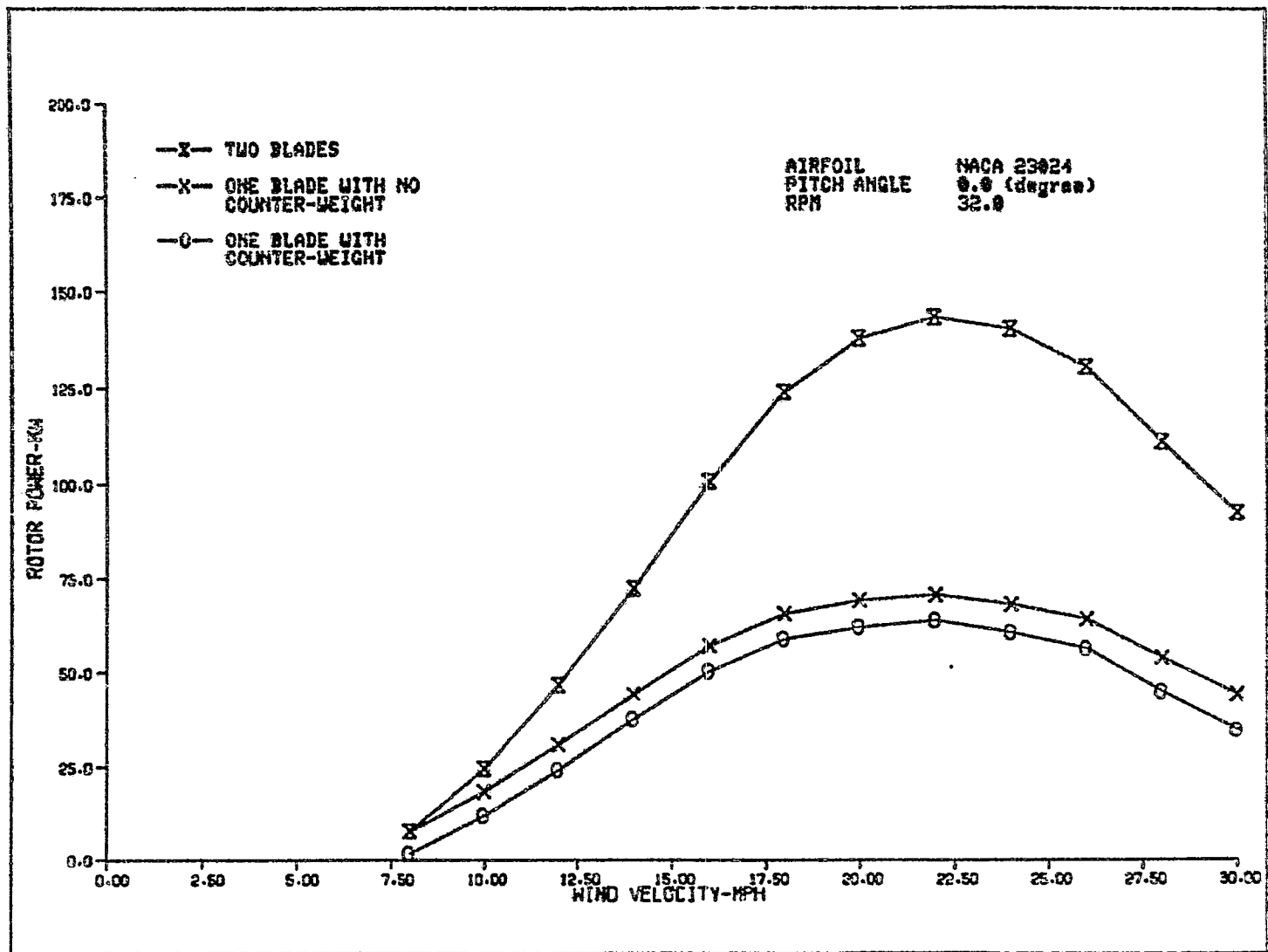
Fig. 3–12 One-bladed rotor concept

Fig. 3-13 Counter-weight and support spar for one bladed rotor

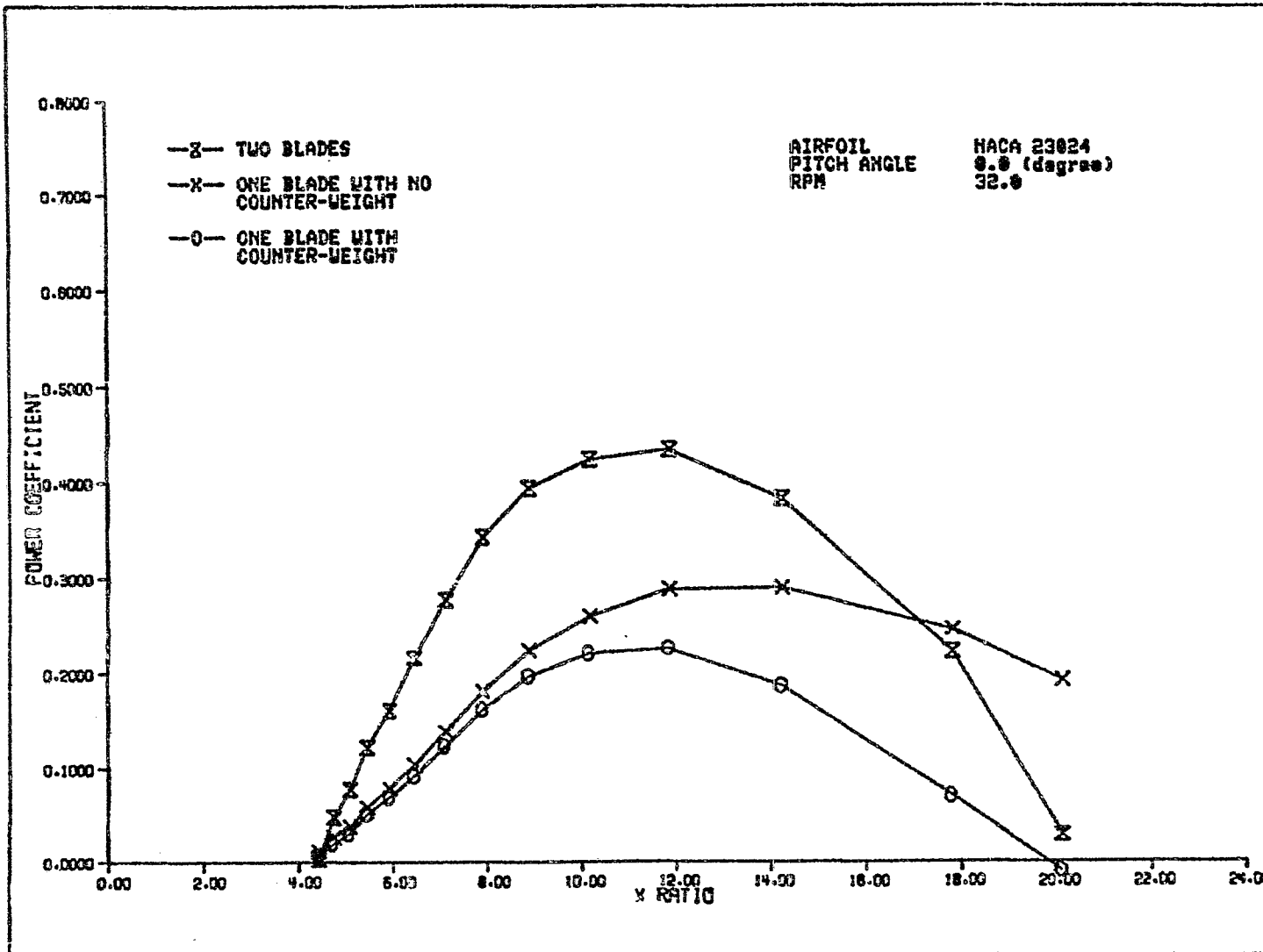Fig. 3-14 ROTOR POWER US. WIND VELOCITY FOR A FIXED PITCH ROTOR

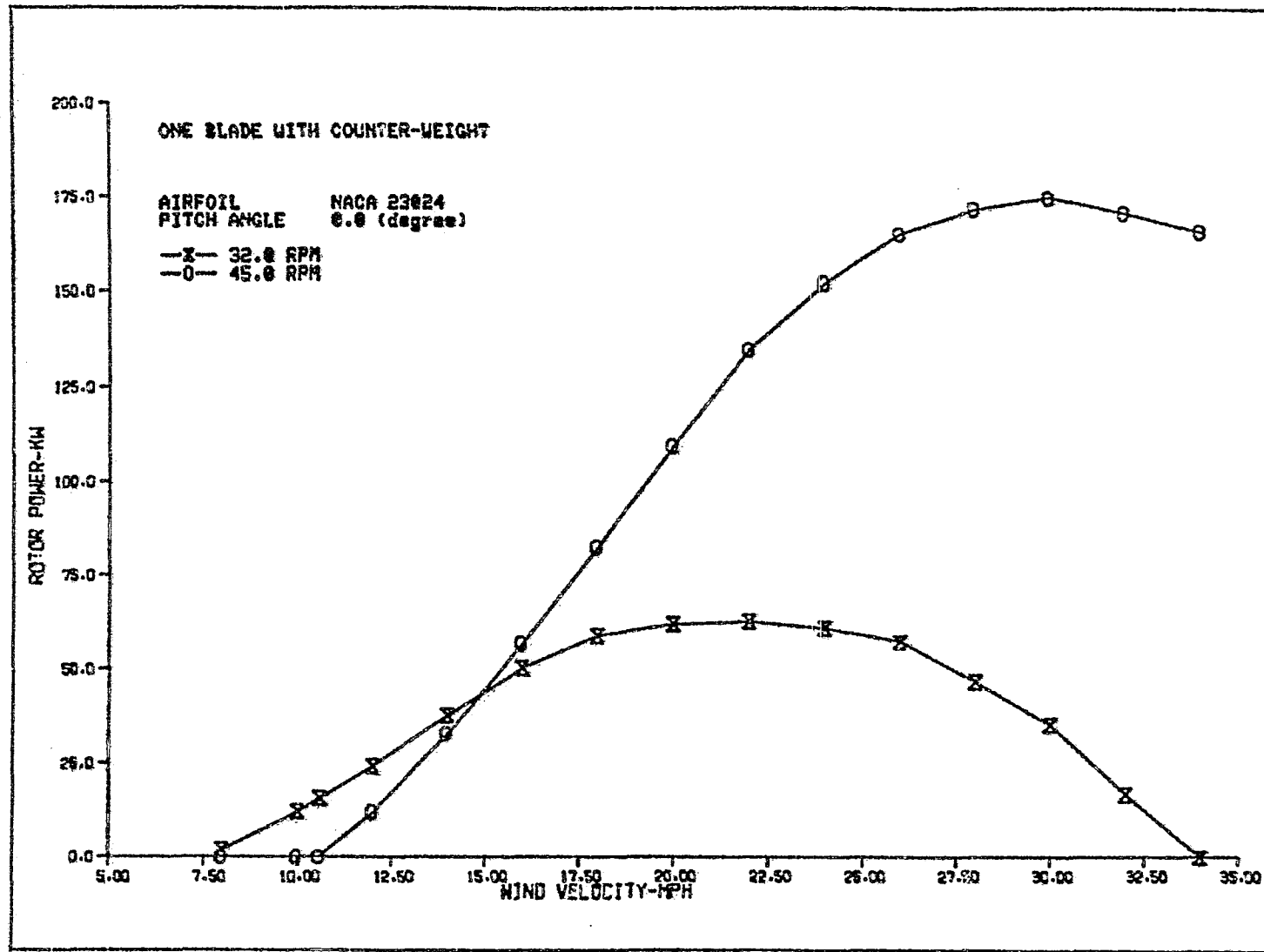Fig. 3-15 POWER COEFFICIENT VS. X RATIO FOR A FIXED PITCH ROTOR

Fig. 3-16 ROTOR POWER VS. WIND VELOCITY FOR A ONE-BLADED FIXED PITCH ROTOR

4. CONCLUSION

In this report, a method for the prediction of wind turbine performance has been developed. The equations presented are fairly general: applicable to any blade geometry or any airfoil section. Although calculations were presented for only one and two bladed rotors, the method is applicable to wind turbines having any number of blades.

The current method has been programmed on a high speed, digital computer to permit extensive analysis. Two-dimensional airfoil data was used as input to the program. This input data can be extended to include variations in Reynolds number and blade surface roughness, and therefore, can enable the computer program to better predict the performance of a blade element. Further refinement of the computer method may be required to take into account an expanding wake and a non-uniform wind velocity. Moreover, a more suitable function for representing the circulation distribution than that used in this investigation may be warranted. The disadvantage of the Fourier series expansion that was used is that the computing time increases sharply as the number of terms increases. Unfortunately, extensive comparison of predicted wind turbine performance was not possible because of the unavailability of accurate data. Such a comparison will be made in the future, as soon as the data are available, and the results will be reported in Volume III of this report.

It was predicted that large losses occur for a one-bladed wind turbine. And, that the peak power of a two-bladed rotor is approximately 50% higher than that of one-bladed rotor operating at a particular rotational speed. However, by increasing the diameter, the same peak power of a two-bladed turbine may be obtained for a one-bladed turbine and may still be economically competitive with a turbine having more blades.

REFERENCES

1. Wilson, R. E. and Walker, S. N. "A Fortran Program for the Determination of Performance, Load and Stability Derivatives of Windmills," Department of Mechanical Engineering, Oregon State University (RAAN), Under Grant No. GI-41840, Oct. 25, 1974.

2. Wilson, R. E. and Lissaman, P. B. S. "Applied Aerodynamics of Wind Power Machines," U. S. Department of Commerce, National Technical Information Service, P. B. -238-595.

3. R. H. Miller, et al "Aerodynamics of Horizontal Axis Wind Turbines" Wind Energy Conversion Volume 2, MIT Report. Coo-4131-T1, U.S. Department of Commerce. National Technical Information Center.

4. Richards, T. "Mod-0 Performance," PIR No. 11, NASA Lewis Research Center, Cleveland, Ohio, 1977.

5. Viterna, L. "Mod-0 Utility Pole Blade Performance," PIR No. 109, NASA Lewis Research Center, Cleveland, Ohio, 1979.

6. Moriya, T. "Selected Scientific and Technical Papers," University of Tokyo, 1959.

7. Keathe, A. N. and Schetzer, T. D. Foundation of Aerodynamics, 3rd edition, John Wiley, 1957.

8. McCormick, B. W. Aerodynamics of V/STOL Flight, Academic Press, Ne New York, 1967.

9. Durrand, W. F. Aerodynamic Theory, Vol. IV, Dover Press, 1945.

10. Goldstein, S. "On the Vortex Theory of Screw Propellers," Proceeding of the Royal Society of London, Series A, Vol. 123, 1923.

11. Theodorson, T. Theory of Propellers, McGraw-Hill, 1948.

12. Neustadter, H. and Wolf, R. "Mod-O Hard and Soft Tower; Utility Pole Blades Power, Flap Bending, Chord Bending and Horizontal Acceleration," PIR No. 106, NASA Lewis Research Center, Cleveland, Ohio, 1979.

13. Pawlas, G. E., Miller, D. R. and Viterna, L. "Effect of Pitch Angle on Wind Turbine Performance Below Rated Wind Speed," PIR No. 149 NASA Lewis Research Center, Cleveland, Ohio, 1980.

14. Rankine, W. J. M. "On the Mechanical Principle of the Action of Propellers," Transaction of the Institute of Naval Architects, Vol. 6, 1865.

15. Froude, W. "On the Elementary Relation Between Pitch, Slip and Propulsive Efficiency," Transaction of the Institue of Naval Architects, Vol. 19, 1878.

16. Glauert, H. The Element of Airfoil and Airscrew Theory, University Press, Cambridge, 1948.

17. Prandtl, L. "Application of Modern Hydrodynamics to Aeronautics," NACA Report 116, 1921.

18. Betz, A. Aerodynamic Theory, edited W. F. Durrand, Vol. IV, Div. I, Dover Press, 1945.

19. Lock, C. N. H. "The Application of Goldstein Theory to the Practical Design of Airscrews," Aeronautical Research Committee, Report and Memoranda No. 1377, 1930.

APPENDIX A

Review of Various Methods of Wind Turbine Aerodynamic Performance

Calculation

Review of Various Methods of Wind Turbine Aerodynamic Performance Calculation

The purpose of this Appendix is to briefly present some of the theoretical background for a variety of the methods that have been used to predict the aerodynamic performance of horizontal axis wind turbines. It should be mentioned that this review is not comprehensive, for such an undertaking would far exceed the practical limits of this work. The methods which will be described herein are: momentum theory, blade element theory, Glauert Vortex theory, Prandtl theory and Goldstein theory.

I. Momentum Theory

In the original, so-called, momentum theory developed by Rankine [14] and Froude [15], momentum and energy principles are applied to a simplified model that is based on the following three assumptions:

1) The thrust loading is uniformly distributed over the propeller disk (this implies that there are an infinite number of blades in the disk).

2) No rotation is imparted to the flow.

3) A well-defined slipstream separates the flow passing through the propeller disk from that outside the disk.

The momentum theorem is applied to the control volume shown in Fig. A-1 and it is found that

$$F = \dot{m}(V_0 - V_2) = \rho A U(V_0 - V_2) \tag{A-1}$$

In this equation, F is the axial force on the wind turbine, $\dot{m}$ is the flow rate, V_0 is the freestream velocity and the V_2 is downstream velocity. Also, density, area and velocity at the rotor disk are denoted by ρ, A and U, respectively.
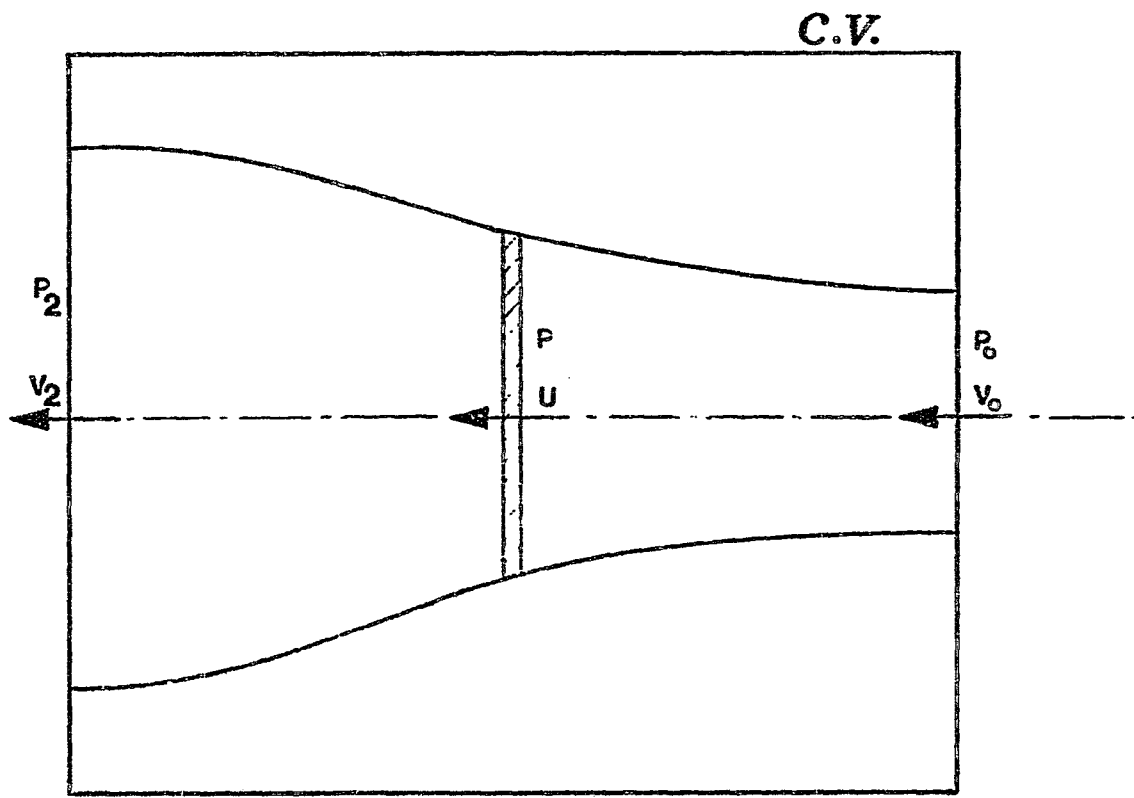
Fig. A—1 The flow field and control volume for momentum theory

If Δp is the discontinuous decrease in the static pressure across the rotor disk, then the axial force on rotor may be expressed as

$$F = A\Delta p$$

An expression for Δp can be obtained by applying Bernoulli's equation in front of and behind the rotor disk

$$p_0 + \frac{1}{2} \rho V_0^2 = p + \frac{1}{2} \rho U^2$$

$$p_0 + \frac{1}{2} \rho V_2^2 = p + \frac{1}{2} \rho U^2 - \Delta p$$

Subtraction and rearrangement brings

$$\Delta p = \frac{1}{2} \rho (V_0^2 - V_2^2)$$

Therefore, the axial force on the wind turbine is

$$F = A\Delta p = \frac{1}{2} \rho A (V_0^2 - V_2^2)$$

Uniting this equation with equation (A-1) results in

$$U = \frac{1}{2} (V_0 + V_2) \qquad (A-2)$$

Thus, the velocity of flow through the disk is the arithmetic average of the upstream and downstream velocities.

An axial interference factor, a, is defined as the fractional change in the freestream velocity that occurs ahead of the disk, i.e.,

$$a = \frac{V_0 - U}{V_0}$$

Hence, the velocity of flow through the disk may be written

$$U = V_0(1 - a) \qquad (A-3)$$

Equating equations (A-2) and (A-3) and rearranging reveals that

$$a = \frac{V_0 - V_2}{2V_0} = \frac{1}{2} - \frac{V_2}{2V_0} \tag{A-4}$$

And it may be seen that when the rotor absorbs all the energy of the flow ($V_2 = 0$), the interference factor will have a value of 1/2.

The power absorbed by the rotor is equal to the mass flow rate times the change in kinetic energy of the incoming fluid, i.e.,

$$P = \frac{1}{2} \rho A U (V_0^2 - V_2^2) \tag{A-5}$$

Combining equations (A-2), (A-4) and (A-5), yields

$$P = 2\rho A V_0^3 a(1 - a)^2 \tag{A-6}$$

It can be seen that for a given wind speed, rotor size and air density, the power absorbed depends only on the interference factor. Hence, maximum power is produced when $\frac{dP}{da} = 0$. It is easy to show that this condition occurs for an axial interference value of $\frac{1}{3}$. Thus, from (A-6)

$$P_{max} = \frac{16}{27} (\frac{1}{2} \rho A V_0^3) = 0.593(\frac{1}{2} \rho A V_0^3) \tag{A-7}$$

and a power coefficient, defined as

$$C_p = \frac{P}{\frac{1}{2} \rho A V_0^3} \tag{A-8}$$

has a maximum value of 0.593.

If the rotation imparted to flow is included, in the analysis, the total reduction in translational kinetic energy of the flow is

$$\Delta K.E. = \text{Power Extracted} + \text{Rotation K.E.}$$

Therefore, in order to obtain the maximum power from the stream, it is necessary to keep the rotational kinetic energy as small as possible. Moreover, the element of torque is equal to the angular momentum imparted to the blade element in unit time. This equation for a blade element at radial distance r, if Ω_W is the rotational velocity of the air, can be written as

$$dQ = 2\pi r^3 \rho U \Omega_W dr \tag{A-9}$$

An angular interference factor is defined as

$$a' = \frac{\Omega_W}{2\Omega} \tag{A-10}$$

where Ω is the rotational velocity of the blade. Introducing equation (A-10) into equation (A-9) yields

$$dQ = 4\pi r^3 \rho U\ a'\Omega dr \tag{A-11}$$

Using this equation along with the previous theory, allows the incremental axial force, torque and power to be written respectively as

$$dF = 4\pi r \rho V_0^2\ a(1 - a)dr \tag{A-12}$$

$$dQ = 4\pi r^3 \rho V_0(1 - a)a'\Omega dr \tag{A-13}$$

$$dP = 4\pi r^3 \rho V_0(1 - a)a'\Omega^2 dr \tag{A-14}$$

It should be mentioned that momentum theory provides a good indication of the power coefficient, but fails to furnish the required design data for the rotor blades except for the limiting case of an infinite number of blades.

II. Blade Element Theory

An alternate method of analyzing the behavior of a blade consists of directly estimating the forces experienced by the blade due to the motion of the air. This method, generally referred to as blade element theory [9], is based on the assumption that the aerodynamic force acting on the blade element can be estimated as the force on a suitable airfoil of the same cross-section in an airflow with a uniform velocity W at the same angle of attack. And, that the force on the entire blade can be derived by summing the contributions of all the elements along the blade. From the velocity and force diagram for a blade element shown in Fig. A-2, it can be seen that

$$\tan\phi = \frac{V_0}{r\Omega} \tag{A-15}$$

where ϕ is the angle between the resultant velocity and free stream velocity. In addition, the incremental axial force and torque are
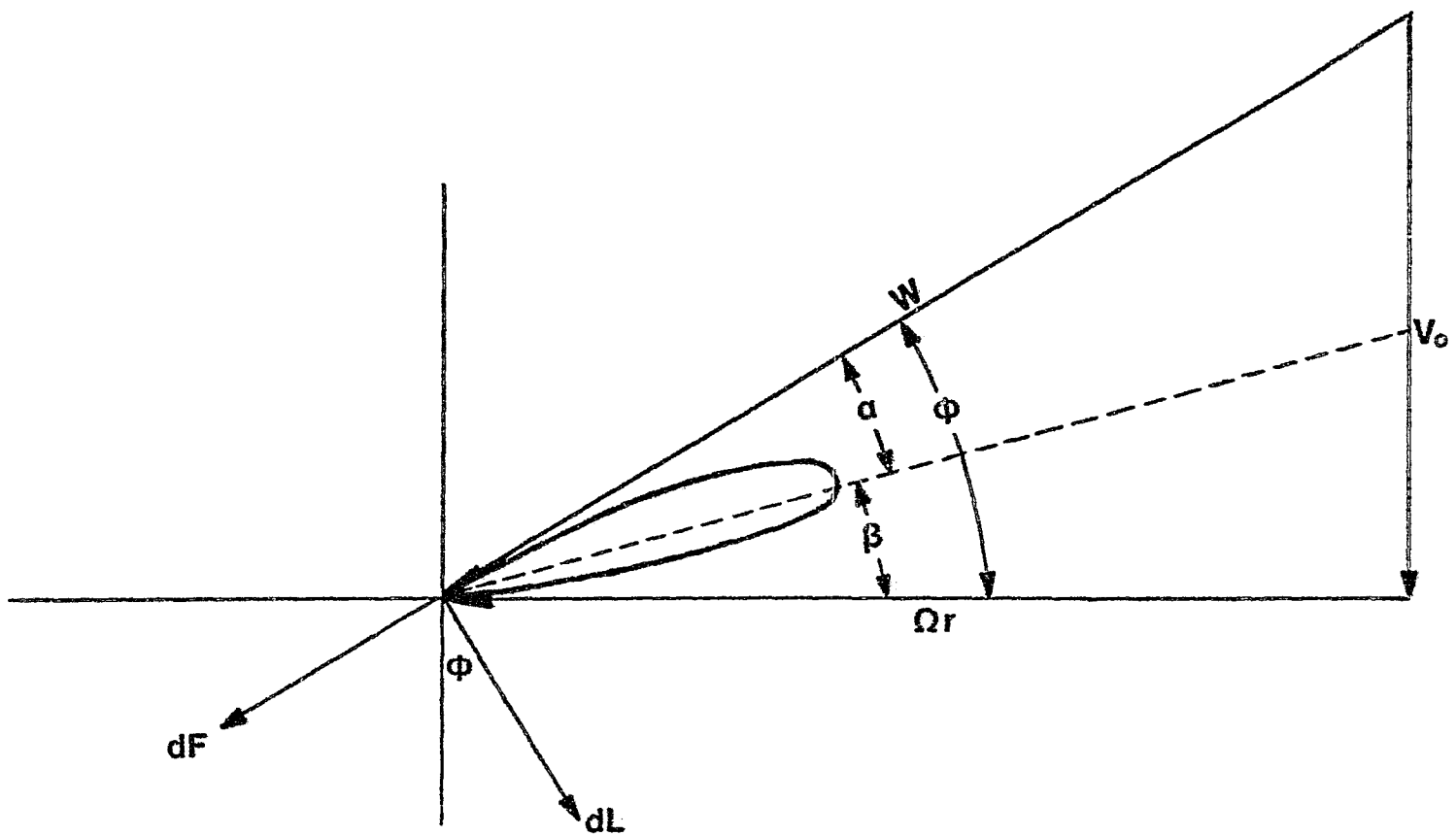
$$dF = \frac{1}{2} NcW^2(C_L\cos\phi + C_D\sin\phi)dr \tag{A-16}$$

$$dQ = \frac{1}{2} NcW^2(C_L\sin\phi - C_D\cos\phi)dr \tag{A-17}$$

where c is the chord of blade element, N is the number of blades and the lift and drag coefficients are

$$C_L = \frac{dL}{\frac{1}{2}\rho w^2 c\ dr} \tag{A-18}$$

$$C_D = \frac{dD}{\frac{1}{2}\rho w^2 c\ dr} \tag{A-19}$$

Fig. A—2 Force and velocity diagram for blade elemet theory

If the section lift and drag coefficients are known, the axial force and torque can be determined by integrating equations (A-16) and (A-17) along the blade. It should be mentioned that the blade characteristics are those of an airfoil of the same cross-section in a two-dimensional airflow.

The unsatisfactory feature of blade element theory is that it relies on certain airfoil characteristics which vary with aspect ratio and which depend on the interference between the adjacent blades of a rotor. Further, this theory using airfoil data corresponding to a moderate blade aspect ratio, has been found to properly represent observed behavior of a propeller, but fails to provide accurate numerical results [9]. To improve the accuracy of blade element theory it has been suggested, [9], that the resultant velocity of the blade should be estimated in terms of modified velocities such as those that were determined by the momentum theory. The combined momentum-blade element theory equations are similar to those of the Glauert Vortex theory, [16] which will be discussed in the following section.

III. Glauert Vortex Theory

Glauert Vortex Theory is based on the assumption that trailing vortices emanate from the trailing edge of rotating blades and form helical vortex sheets that pass downstream. The interference velocity experienced by the blades is calculated as the induced velocity of this vortex system on any blade element. The calculation of these induced velocities is simplified by assuming that the rotor has an infinite number of blades. This assumption removes the complexity associated with the periodicity of the flow and permits the momentum theory to be directly used to evaluate the interference velocities. For an element of blade shown in Fig. A-3

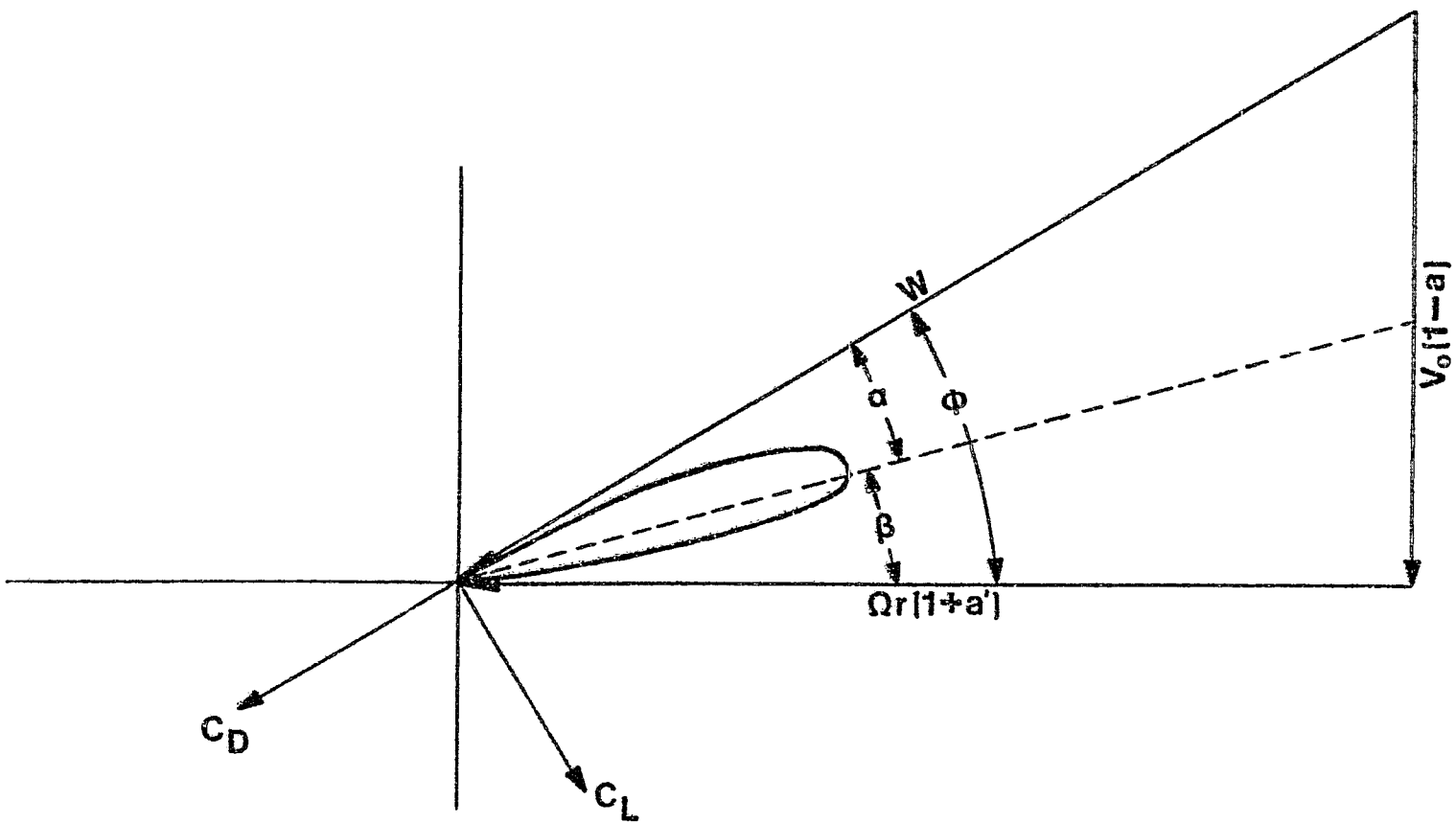$$W \sin\phi = V_0(1 - a)$$

$$W \cos\phi = \Omega r(1 + a')$$

Fig. A—3 Force and velocity diagram for Glauert vortex theory

Thus, the speed ratio is

$$\lambda_0 = \frac{V_0}{R\Omega} = \frac{r}{R} \frac{1 + a'}{1 - a} \ Tan\phi \tag{A-20}$$

where a and a' are axial and rotational interference factors respectively. The incremental axial force and torque in non-dimensional form can be written, using equations (A-16) and (A-17), as

$$dF_c = \frac{\sigma}{R} \ (\frac{W}{V_0})^2 (C_L \ cos\phi + C_D sin\phi) \ dr \tag{A-21}$$

$$dQ_c = \frac{\sigma}{R} \ (\frac{W}{V_0})^2 (\frac{r}{R})(C_L \ sin\phi - C_D cos\phi) \ dr \tag{A-22}$$

where

$$dF_c = \frac{dF}{\rho(\pi R^2) \ V_0^2} \tag{A-23}$$

$$dQ_c = \frac{dQ}{\rho(\pi R^2) \ V_0^2 \ R} \tag{A-24}$$

and σ, solidity ratio, is defined as

$$\sigma = \frac{N_c}{2\pi R} \tag{A-25}$$

In order to solve equations (A-21) and (A-22), ϕ, and the interference factors must first be determined. As an aid to this process, it may be assumed that there is an infinite number of blades, thus, momentum theory equations can be directly applied. In addition, if the rotation in the slipstream is neglected the following relationship is obtained from (A-12), (A-21) and (A-23)

$$\frac{a}{1 - a} = \frac{\sigma_L (C_L \ cos\phi + C_D \ sin\phi)}{4 \ sin^2\phi} \tag{A-26}$$

where σ_L, local solidity, is defined as

$$\sigma_L = \frac{N_C}{2\pi r}$$

Moreover, equating (A-13) with the element of torque obtained by combining (A-22) and (A-24), it is easy to show that

$$\frac{a'}{1 - a'} = \frac{\sigma_L(C_L \sin\phi - C_D \cos\phi)}{4 \sin\phi \cos\phi} \qquad (A-27)$$

These equations strictly apply to a rotor with a large number of blades since the momentum theory equations have been employed. An approximate method of correcting equations (A-26) and (A-27) to account for a rotor with a small number of blades is analogous to that used by Prandtl [17]. According to that method, the distribution of vortex strength over the blade is related to the shape and motion of the airscrew. The relation of the distribution of vortex strength to the velocity field produced by it has been determined by Goldstein [10] for optimum loading. It should also be mentioned that the Glauert Vortex theory does not account for the loss of lift toward the tips of the blades. However, for this theory the concept of an effective radius may be used to account for this loss.

IV. Prandtl Theory

For the optimum circulation condition, the vortex sheet is assumed to be a rigid helical surface moving backward with constant velocity [18]. Near the boundary of the surface there is flow around the edges of the vortex sheet and thus, the flow acquires an important radial component of velocity. Prandtl approximated the effect of this radial flow by replacing the helical vortex system, shown in Fig. A-4, with a series of parallel lines at a
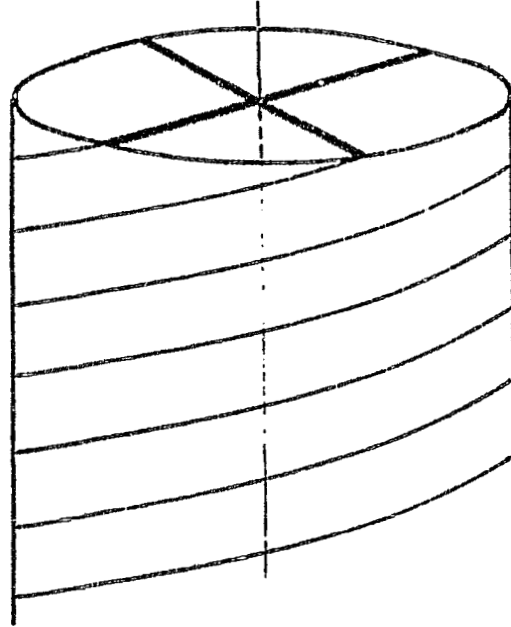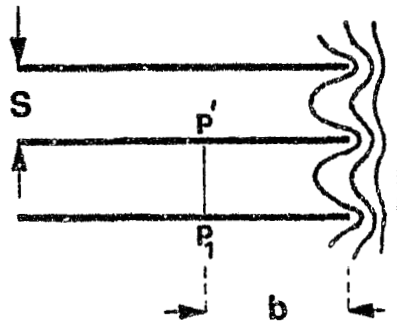
Fig. A—4 Idealized vortex system

Fig. A—5 Transformation representation

regular gap S and extending infinitely to the left as shown in Fig. A-5. The gap S represents the normal distance, at the boundary of the slipstream, between the successive vortex sheets and can be written as

$$S = \frac{2\pi R}{N} \frac{\lambda_0}{(1 + \lambda_0^2)^{1/2}}$$

(A-28)

where

$$\lambda_0 = \frac{V_0}{R\Omega}$$

Prandtl showed that if the rigid vortex system moves downward with a velocity w_0, the mean downward velocity on the line $\overline{P'P_1}$ at a distance b from the edge of the lines (Fig. A-5) becomes

$$\bar{v} = \frac{2}{\pi} w_0 \cos^{-1} (e^{-\pi b/S})$$

Letting

$$F' = \frac{\bar{v}}{w_0} = \frac{2}{\pi} \cos^{-1} (e^{-\pi b/S})$$

F' can be interpreted as the fraction of velocity w_0 which is imparted to the flow of section $\overline{P'P_1}$. In the corresponding propeller analogy then F' is defined as

$$F' = \frac{2}{\pi} \cos^{-1} (e^{-f})$$

(A-29)

where

$$f = \frac{\pi b}{S} = \frac{N}{2} \frac{R - r}{R} \frac{(1 + \lambda_0^2)^{1/2}}{\lambda_0}$$

(A-30)

Thus, F' is a reduction factor which must be applied to the momentum equation for the flow at radius r, since it represents the fact that only a fraction, F', of the fluid between successive sheets of the slipstream receives the full effect of these sheets [9]. Applying this correction to the earlier analysis of momentum theory i.e., equations (A-12) and (A-13) produces

$$dF = 4\pi r \rho V_0^2 \, a(1-a)F' dr$$

$$dQ = 4\pi r^3 \rho V_0 (1-a)a'\Omega \, F' dr$$

Now combining these equations with those obtained in the blade element theory i.e., equations (A-16) and (A-17) results in

$$\frac{a}{1-a} = \frac{\sigma_L(C_L \cos\phi + C_D \sin\phi)}{4F' \sin^2\phi}$$

$$\frac{a'}{1-a'} = \frac{\sigma_L(C_L \sin\phi - C_D \cos\phi)}{4F' \sin\phi \cos\phi}$$

(A-31)

Furthermore, due to the radial flow near the boundary of the slipstream, there is a drop of circulation which can be represented by an equivalent rotor with infinite number of blades but having the same drag. This equivalent radius of this rotor is given in [9] as

$$\frac{R_e}{R} = 1 - \frac{1.386}{N} \frac{\lambda_0}{(1 + \lambda_0^2)^{1/2}}$$

(A-33)

V. Goldstein Theory

Goldstein [10] solved the problem of potential flow past a body consisting of a finite number of coaxial helicoids of infinite length, but finite radius, moving through an inviscid fluid with constant velocity. Further, the fluid motion is assumed to be irrotational. The results are applied to the case of an ideal airscrew having a finite number of blades and a particular distribution of circulation along the blade for small values of thrust. Goldstein [10] specifically considered Betz's optimum condition [18] corresponding to a rigid helicoid. The essential result of Goldstein's calculation is the determination of the strength of the helical vortex system as a function of radius. If Γ is the circulation around a closed circuit cutting a helicoid at radius r and enclosing the part of the surface outside that radius, then Γ is equal to the discontinuity of the velocity potential across the helicoidal surface at radius r, [9]. Also, $-\dfrac{d\Gamma}{dr}$, is equal to the strength of the vortex sheet or equal to the discontinuity in the radial component velocity u_r through the fluid. The airscrew surface which was considered by Goldstein is defined as

$$\theta - \Omega z/V = 0 \text{ or } , \quad 0 \leq r \leq R \qquad (A-34)$$

where r, θ and z are cylindrical coordinates. The axis Z is along the axis of the airscrew surface. Using the following coordinate transformation

$$\mu = \frac{\Omega r}{V_0} \qquad (A-35)$$

and

$$\xi = \theta - \frac{\Omega z}{V_0} \qquad (A-36)$$

Laplace's equation, namely $\nabla^2 \Phi = 0$, in cylindrical coordinates can be

rewritten as

$$\mu^2 \frac{\partial^2 \Phi}{\partial \mu^2} + \mu \frac{\partial \Phi}{\partial \mu} + (1 + \mu^2) \frac{\partial^2 \Phi}{\partial \xi^2} = 0 \qquad \text{(A-37)}$$

since

$$\frac{\partial^2 \Phi}{\partial r^2} = \left(\frac{\Omega}{V_0}\right)^2 \frac{\partial^2 \Phi}{\partial \mu^2} = \left(\frac{\mu}{r}\right)^2 \frac{\partial^2 \Phi}{\partial \mu^2}$$

$$\frac{\partial^2 \Phi}{\partial \theta^2} = \frac{\partial^2 \Phi}{\partial \xi^2}$$

$$\frac{\partial^2 \Phi}{\partial z^2} = \left(\frac{\Omega}{V_0}\right)^2 \frac{\partial^2 \Phi}{\partial \mu^2} = \left(\frac{\mu}{r}\right)^2 \frac{\partial^2 \Phi}{\partial \mu^2}$$

In reference [19], it is shown that the velocity of the air relative to free
stream velocity between successive sheets at a large distance behind the
rotor is normal to the vortex sheets. Now, if u_z and u_θ are the axial and
circumferential components of velocity, their vectorial sum close to the
surface is equal to the component velocity of the surface normal to itself
i.e.,

$$w_0 \cos\phi = u_z \cos\phi - u_\theta \sin\phi$$

or

$$w_0 \cos\phi = \frac{\partial \Phi}{\partial z} \cos\phi - \frac{\partial \Phi}{r \partial \theta} \sin\phi \qquad \text{(A-38)}$$

for $\xi = 0$ or π and $0 \leq r \leq R$

where w_0 is the velocity of the surface and ϕ is the helix angle.

Noting that

$$\tan\phi = \frac{V_0}{\Omega r}$$

and using this equation together with equations (A-35) and (A-36), it can be

shown that

$$\frac{\partial \Phi}{\partial \xi} = \frac{\mu^2}{1 + \mu^2} \qquad (A\text{-}39)$$

for $\xi = 0$ or π, and $0 \leq r \leq R$

In addition to satisfying equation (A-39), Φ must be a single-valued function of position and its derivative must vanish when r is infinite. Furthermore, Φ must be continuous everywhere except at the screw surface. Goldstein has solved this problem and the solution for the circulation distribution along the blade for any number of blades is given in [9] as

$$\frac{N\Gamma\Omega}{2\pi w_0 V_0} = \frac{\mu^2}{1 + \mu^2} - \frac{8}{\pi} \sum_{m=0}^{\infty} \frac{F_{N,2m+1}(\mu)}{(2m+1)}$$

$$- \frac{2}{\pi} \frac{\mu^2}{1 + \mu^2} \sum_{m=0}^{\infty} \frac{I_{N(m+1/2)} \overline{(m+1/2 \, N_\mu)}}{N(m+1/2) \, \overline{(m+1/2 \, N_{\mu_0})}} \qquad (A\text{-}40)$$

where I functions are the modified Bessel functions and the F functions are computed from

$$F_{N,2m+1}(\mu) = \frac{\mu^2}{1 + \mu^2} - T_{1,N(m+1/2)} \overline{(m+1/2 \, N\mu)} \qquad (A\text{-}41)$$

The T functions appearing in equation (A-41) can be calculated from

$$T_{1,N(m+1/2)} \overline{(m+1/2 \, N_\mu)} = \tau_0(\mu) + \frac{4\tau_2(\mu)}{N^2(2m+1)^2} + \frac{16\tau_4(\mu)}{N^4(2m+1)^4} + \cdots \qquad (A\text{-}42)$$

where

$$\tau_0 = \frac{\mu^2}{1 + \mu^2} \qquad (A\text{-}43)$$

$$\tau_{2r} = \frac{\mu}{1 + \mu^2} \frac{d}{d\mu} \left(\mu \frac{d\tau_r}{d\mu} \right) \qquad (A\text{-}44)$$

so that

$$\tau_2 = 4\mu^2 (1 - \mu^2) / (1 + \mu^2)4 \qquad (A\text{-}45)$$

$$\tau_4 = 16\mu^2 \{ 1 - 14\mu^2 + 21\mu^4 - 4\mu^6 \} / (1 + \mu^2)7 \qquad (A\text{-}46)$$

Goldstein defined a non-dimensional circulation factor as

$$K = \frac{N\Gamma\Omega}{2\pi w_0 V_0} = \frac{N\Gamma}{2\pi w_0 r} \frac{1}{\tan\phi} . \qquad (A\text{-}47)$$

This factor was calculated and plotted [10].

Lock [19] applied Goldstein's solution without restriction to an arbitrary circulation distribution in order to obtain the interference velocities instead of following the standard formula of the Glauert Vortex theory [16]. He showed that the axial and circumferential components of the interference velocity at the rotor plane differs from those of Glauert vortex theory by a factor $\frac{\cos^2\phi}{K}$, if the helix angle in both cases is assumed to be the same. Applying this factor, Lock modified the Glauert Vortex method for the case of a small number of blades.

1. Report No. NASA CR-168054	2. Government Accession No.	3. Recipient's Catalog No.
4. Title and Subtitle Aerodynamic Analysis of a Horizontal Axis Wind Turbine by use of Helical Vortex Theory Volume I - Theory		5. Report Date December 1982
		6. Performing Organization Code
7. Author(s) D. R. Jeng, T. G. Keith, Jr., and A. Aliakbarkhanafjeh		8. Performing Organization Report No.
		10. Work Unit No.
9. Performing Organization Name and Address University of Toledo Dept. of Mechanical Engineering Toledo, Ohio 43606		11. Contract or Grant No. NCC 3-5
		13. Type of Report and Period Covered Contractor Report
12. Sponsoring Agency Name and Address U.S. Department of Energy Wind Energy Technology Division Washington, D.C. 20545		14. Sponsoring Agency Code Report No. DOE/NASA/0005-1

16. Abstract

The theoretical development of a method of analysis for prediction of the aerodynamic performance of horizontal axis wind turbines is presented in this report. The method is based on the assumption that a helical vortex emanates from each blade element. Collectively these vortices from a vortex system that extends infinitely far downstream of the blade. Velocities induced by this vortex system are found by applying the Biot-Savart law. Accordingly, this method avoids the use of any interference factors which are used in many of the momentum theories. What's more, the method can be used to predict the performance of wind turbines with a small number of blades. The wind turbine performance of a two-bladed rotor is determined and compared to existing experimental data and to corresponding values computed from the widely used PROP code. It was found that the present method compared favorably with experimental data especially for low wind velocities. The wind turbine performance of a single-bladed rotor is determined subject to the condition that there was no lift on the counterweight or support span. Output power for a one-bladed wind turbine was compared to that of a two-bladed machine.

17. Key Words (Suggested by Author(s)) Wind turbine aerodynamics Helical vortex theory	18. Distribution Statement
19. Security Classif. (of this report) Unclassified	20. Security Classif. (of this page) Unclassified	21. No. of pages 85	22. Price*